Lithos 240–243 (2016) 202–227

Contents lists available at ScienceDirect

Lithos

journal homepage: www.elsevier.com/locate/lithos

Cobalt and precious metals in sulphides of peridotite xenoliths and inferences concerning their distribution according to geodynamic environment: A case study from the Scottish lithospheric mantle

Hannah S.R. Hughes [a,*], Iain McDonald [a], John W. Faithfull [b], Brian G.J. Upton [c], Matthew Loocke [a]

[a] School of Earth and Ocean Sciences, Cardiff University, Main Building, Cardiff CF10 3AT, UK
[b] Hunterian Museum and Art Gallery, University of Glasgow, Glasgow G12 8QQ, UK
[c] School of Geosciences, University of Edinburgh, Edinburgh EH9 3JW, UK

ARTICLE INFO

Article history:
Received 12 February 2015
Accepted 1 November 2015
Available online 12 November 2015

Keywords:
North Atlantic Craton
Mantle xenolith
Cobalt
PGE
Sulphide

ABSTRACT

Abundances of precious metals and cobalt in the lithospheric mantle are typically obtained by bulk geochemical analyses of mantle xenoliths. These elements are strongly chalcophile and the mineralogy, texture and trace element composition of sulphide phases in such samples must be considered. In this study we assess the mineralogy, textures and trace element compositions of sulphides in spinel lherzolites from four Scottish lithospheric terranes, which provide an ideal testing ground to examine the variability of sulphides and their precious metal endowments according to terrane age and geodynamic environment. Specifically we test differences in sulphide composition from Archaean-Palaeoproterozoic cratonic sub-continental lithospheric mantle (SCLM) in northern terranes *vs.* Palaeozoic lithospheric mantle in southern terranes, as divided by the Great Glen Fault (GGF).

Cobalt is consistently elevated in sulphides from Palaeozoic terranes (south of the GGF) with Co concentrations > 2.9 wt.% and Co/Ni ratios > 0.048 (chondrite). In contrast, sulphides from Archaean cratonic terranes (north of the GGF) have low abundances of Co (<3600 ppm) and low Co/Ni ratios (<0.030). The causes for Co enrichment remain unclear, but we highlight that globally significant Co mineralisation is associated with ophiolites (e.g., Bou Azzer, Morocco and Outokumpu, Finland) or in oceanic peridotite-floored settings at slow-spreading ridges. Thus we suggest an oceanic affinity for the Co enrichment in the southern terranes of Scotland, likely directly related to the subduction of Co-enriched oceanic crust during the Caledonian Orogeny. Further, we identify a distinction between Pt/Pd ratio across the GGF, such that sulphides in the cratonic SCLM have Pt/Pd ≥ chondrite whilst Palaeozoic sulphides have Pt/Pd < chondrite. We observe that Pt-rich sulphides with discrete Pt-minerals (e.g., PtS) are associated with carbonate and phosphates in two xenolith suites north of the GGF. This three-way immiscibility (carbonate-sulphide-phosphate) indicates carbonatitic metasomatism is responsible for Pt-enrichment in this (marginal) cratonic setting. These Co and Pt-enrichments may fundamentally reflect the geodynamic setting of cratonic *vs.* non-cratonic lithospheric terranes and offer potential tools to facilitate geochemical mapping of the lithospheric mantle.

1. Introduction

The lithospheric mantle has variably undergone complex magmatic and metasomatic events, dependent upon the age, structure and transient geodynamic environment(s) recorded in any one region. The sub-continental lithospheric mantle (SCLM) as a source of metals has been studied for decades (e.g., Groves and Bierlein, 2007; Groves et al., 1987; Rock and Groves, 1988 and references therein) but recent interest in how the SCLM relates to metals of strategic and economic importance has invigorated this discussion (e.g., Arndt, 2013). For example, platinum-group elements (PGE) and cobalt are designated 'critical metals' in various political reports, summarised by Gunn (2014). Many such metals have a strong affinity to sulphur, and hence the ability of the shallow mantle to store or release these elements is largely dependent on the nature of the sulphur budget — i.e., the abundance of sulphur, if this sulphur exists as sulphide or sulphate, and the petrological sighting of sulphide minerals (interstitial to silicates *vs.* mineral inclusions).

Studies of the noble metal and chalcophile element composition of the lithospheric mantle (as sampled by mantle xenoliths in dykes and pipes) can focus on the bulk rock geochemistry and

Abbreviations: NAC, North Atlantic Craton; GGF, Great Glen Fault; NAIP, North Atlantic Igneous Province; BPIP, British Palaeogene Igneous Province; SCLM, subcontinental lithospheric mantle; PGE, platinum-group elements; MSS, Monosulphide solid solution.

* Corresponding author at: School of Geosciences, University of the Witwatersrand, Private Bag 3, Wits 2050, Johannesburg, South Africa. Tel.: +27 11 717 6547.
E-mail address: hannah.hughes@wits.ac.za (H.S.R. Hughes).

http://dx.doi.org/10.1016/j.lithos.2015.11.007

isotopic compositions (e.g., Re–Os) of xenoliths (see Lorand et al., 2013 and references therein; Ionov et al., 2015). But consideration should also be given to the mineralogical and textural setting of sulphides (e.g., Delpech et al., 2012; Warren and Shirey, 2012 and references therein; Lorand et al., 2013 and references therein; Hughes, 2015). These influence the capacity of sulphides to release critical metals under different melting regimes. Further, textural and isotopic evidence regarding the age and potential origin of these sulphides (e.g., metasomatic Pd-Cu–Ni rich sulphides *vs.* residual metal alloys and base metal sulphides after melt depletion) may provide deeper insights into the lithospheric mantle metal budget (Delpech et al., 2012; Lorand et al., 2013).

Cobalt has generally been neglected in xenolith studies and other mantle investigations (cf. Pearson, 2005), however as we show in this investigation, Co may be particularly illuminating in 'fingerprinting' some geodynamic regimes, such as oceanic plate subduction. This may largely be because the bulk geochemistry of Co in xenoliths is predominantly controlled and buffered by high modal abundances of Co-bearing silicates, such as olivine (Co concentration 87–143 ppm in $Fo_{89.3–93.3}$ within mantle peridotite xenoliths (De Hoog et al., 2010) and 170–220 ppm in $Fo_{80.6–87.7}$ within basalts (Søager et al., 2015)) rather than low-abundance sulphides. Hence bulk analysis may not be sensitive enough to identify mineralogical enrichments in both precious metals and Co. Classification schemes for mantle-derived magmas have recently been constructed using the abundance and fractionation of Co (e.g., Hastie et al., 2007, 2008). These are based on the strong partitioning of Co into olivine, and Co is thought to be immobile during surficial alteration and weathering of lavas, as demonstrated by laterite profiles over ultramafic terranes (Hastie et al., 2007 and references therein). However, Co is known to be concentrated along with a suite of other metals in seafloor hydrothermal mineralisation settings, for example at mid-ocean ridges (e.g., Von Damm, 2013), particularly ultramafic-hosted massive sulphides at slow-spreading ridges (Bogdanov et al., 1997; Douville et al., 2002; Murphy and Meyer, 1998). Hence at present we have a limited understanding of the geochemical behaviour of Co, and considering its status as a critical metal, it would be advantageous to study its metallogenesis and tectonic regimes that may result in its mineralisation.

For the metallogenesis of a mantle region, and magmas derived from that region, the petrographic siting of sulphides and their composition are key controls, and this may be reflected in mineralisation at the surface (e.g., Hughes et al., 2015a). For example, it can be demonstrated in lavas of the North Atlantic Igneous Province that changes in Pt/Pd bulk rock ratio are a result of contamination by shallow marginal cratonic SCLM-derived sulphides which have elevated Pt abundances. Hence the earliest lavas of this region that intruded up through cratonic SCLM have the highest Pt/Pd ratios, whilst younger lavas see a gradual decrease in Pt/Pd ratio (Hughes et al., 2015a). In this investigation we envisage that a similar compositional control for mantle-derived magmas may be noted for Co (i.e., reflecting Co-rich or Co-poor SCLM sulphides per lithospheric terrane).

During mantle melting, some of the first mineral phases to melt are sulphides, alongside garnet and clinopyroxene (and later incorporating orthopyroxene, spinel and olivine — see Pearson et al., 2003 and references therein). Thus, with increasing degrees of partial melting the amount of sulphur in the melt increases until no sulphides remain in the mantle source region. Complications to this model may be added depending on whether an equilibrium batch melting, fractional melting, continuous melting, or dynamic melting model is assumed (e.g., Rehkamper et al., 1999). However, assuming a starting S concentration of 200 ppm, or 550 ppm Fe-sulphide, in an equilibrium batch melting system (Palme and O'Neill, 2004) all sulphides present in the source will have been completely dissolved in the silicate magma by 13.5% partial melting (Li and Ripley, 2009; Naldrett, 2011). Beyond this point, continued melting only dilutes the S concentration as further S-poor melt is generated. This is the opposite to MgO, which continues to increase with increasing degrees of partial melting, due to the continued melting of clinopyroxene, orthopyroxene, and eventually olivine and spinel. Hence a peak in S concentration (*vs.* percentage partial melting) has repercussions for the concentrations of chalcophile elements such as Ni, Cu, Co and PGE in silicate magmas and the residual mantle source.

Cobalt has similar sulphide solid/sulphide liquid partition coefficients as Ni so that there is no discernible fractionation between these elements during crystallisation of sulphide liquids or separation of liquid from residual sulphide under various P-T conditions (e.g., Ballhaus et al., 2001; Li et al., 1996; Ohtani et al., 1997). However between sulphides and silicates, $D_{sulphide/silicate}$ values for Ni and Co decrease with increasing pressure and temperature, and this effect is greater for Ni than Co (e.g., Ballhaus et al., 2001, Li and Agee, 1996). Thus, when discussing the sulphide-bearing lithospheric mantle, sulphide minerals play a key role in controlling the release of Co to silicate magmas. Despite this, Co abundances in sulphides are remarkably underreported in the literature (with the notable exceptions of Aulbach et al., 2004; Davies et al., 2004 and Wang et al., 2010).

In this study we present new whole-rock and *in situ* sulphide geochemical data for precious metals and chalcophile elements of Scottish mantle xenoliths from terranes north and south of the Great Glen Fault (GGF). Scotland is an ideal place to investigate variations in mantle xenoliths as the Scottish terranes record a range of geodynamic environments; from the margin of the Archaean North Atlantic Craton (north of the GGF) to collided Palaeozoic arcs and associated lithosphere (south of the GGF). Furthermore, Scotland as a whole has experienced several intra-plate rifting events. We consider the geochemistry of mantle sulphide minerals (particularly for Co) in this geodynamic context.

2. Geological setting

2.1. Scottish terranes

Scotland is divided into five tectonic terranes by major lithospheric lineaments (Fig. 1a), the most significant of these being the Great Glen Fault (GGF). The GGF was initiated during the Scandian event of the Caledonian Orogeny (motion between Laurentia and Baltica; Dewey and Strachan, 2003) and now essentially separates two terranes in the north (Hebridean and Northern Highland Terranes) which are underlain by Archaean–Palaeoproterozoic basement of the North Atlantic Craton (locally known as the Lewisian Gneiss Complex), from three younger terranes (from north to south; the Grampian, Midland Valley and Southern Upland Terranes).

2.1.1. North of the GGF

In the northwest of Scotland (Hebridean Terrane), the Lewisian Gneiss Complex (a marginal fragment of the North Atlantic Craton which became detached from the main Greenlandic NAC during the opening of the North Atlantic) consists of amalgamated Archaean cratonic domains, reworked during Palaeoproterozoic orogenesis that can be broadly correlated to the Nagssuqtoqidian belt of Greenland — Fig. 1b (Kolb, 2014; van Gool et al., 2002). In summary, the Lewisian Gneiss Complex can be divided according to the following major tectono-magmatic events: (a) magmatic protolith formation (including ultramafic-mafic bodies now preserved as pods within tonalite–trondhjemite–granodiorite (TTG) gneisses) at 3.0–2.8 Ga; (b) high-grade regional metamorphism followed by initiation of shear zones and associated metamorphism at 2.8–2.5 Ga. (c) Intrusion of mafic-ultramafic dykes (Scourie Dykes) c. 2.4–2.3 Ga during a period of continental rifting and extension (Davies and Heaman, 2014); and lastly (d) c. 2.0–1.8 Ga calc-alkaline magmatism and volcanic arc accretion, with formation of Laxfordian metamorphic belts and crustal anatexis (Crowley et al., 2015; Goodenough et al., 2013; Hughes et al., 2014; Kinny et al., 2005; Love et al., 2010; Park, 2005).

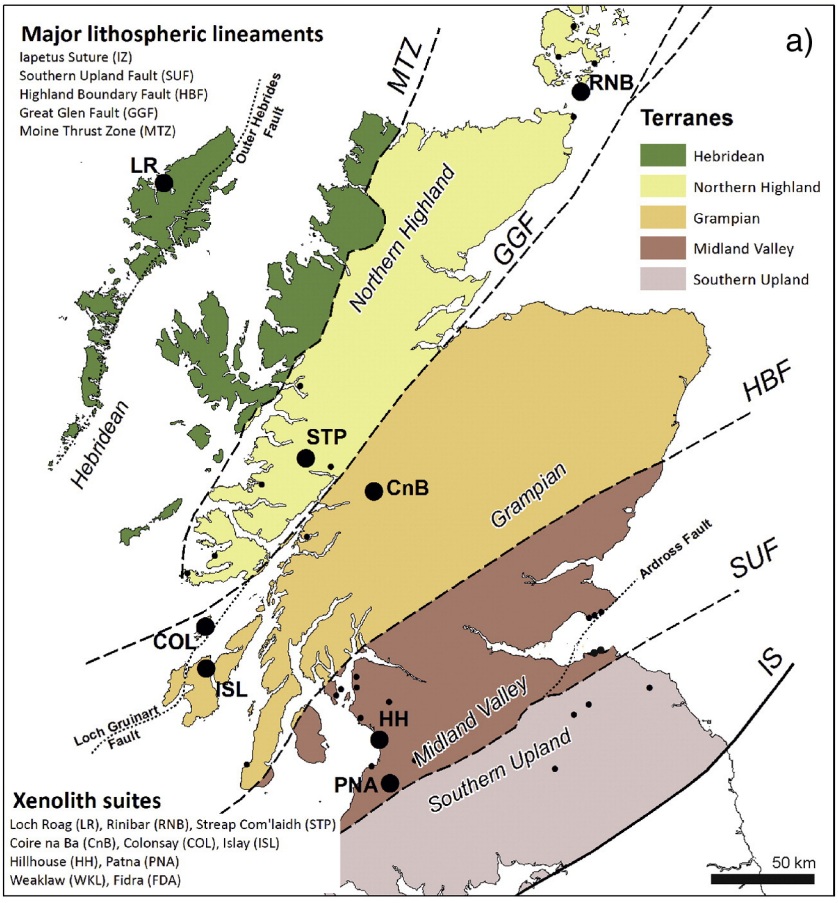
Major lithospheric lineaments
Iapetus Suture (IZ)
Southern Upland Fault (SUF)
Highland Boundary Fault (HBF)
Great Glen Fault (GGF)
Moine Thrust Zone (MTZ)
a)
Terranes
Hebridean
Northern Highland
Grampian
Midland Valley
Southern Upland
MTZ
RNB
LR
Outer Hebrides Fault
Northern Highland
GGF
HBF
STP
CnB
Hebridean
Grampian
Ardross Fault
SUF
COL
ISL
IS
Loch Gruinart Fault
HH
Midland Valley
Southern Upland
PNA
Xenolith suites
Loch Roag (LR), Rinibar (RNB), Streap Com'laidh (STP)
Coire na Ba (CnB), Colonsay (COL), Islay (ISL)
Hillhouse (HH), Patna (PNA)
Weaklaw (WKL), Fidra (FDA)
50 km

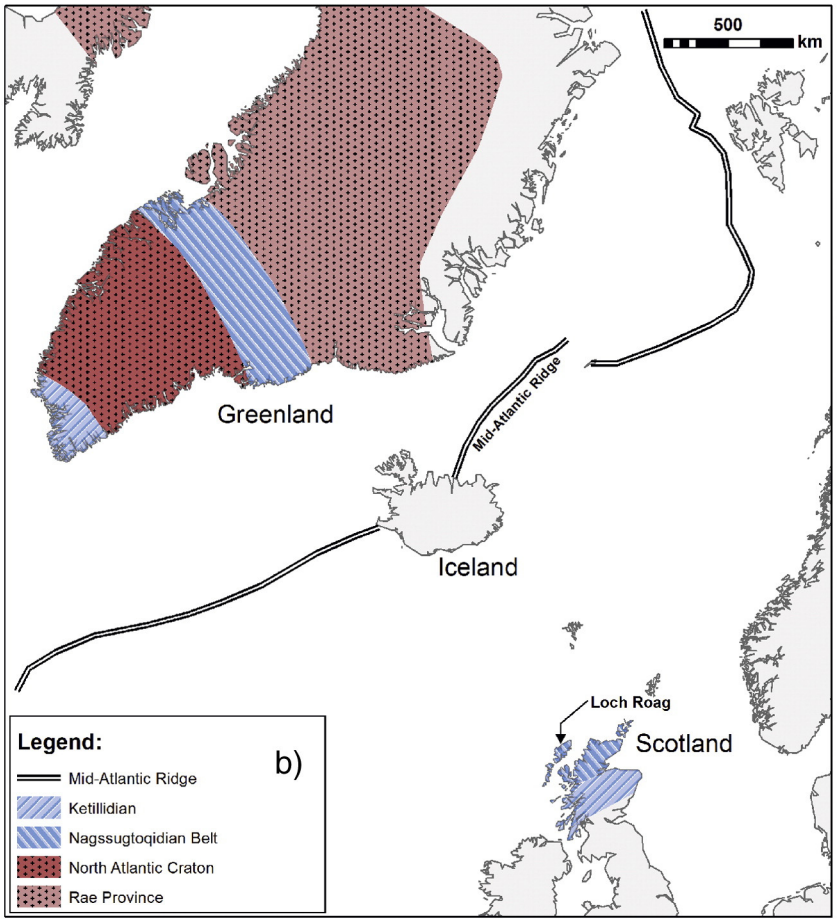
500 km
Greenland
Mid-Atlantic Ridge
Iceland
Loch Roag
Scotland
Legend:
b)
Mid-Atlantic Ridge
Ketillidian
Nagssugtoqidian Belt
North Atlantic Craton
Rae Province

The Lewisian is part of the basement of the Caledonian foreland bounded to the east by the Moine Thrust Zone (MTZ); a thin-skinned thrust zone which delineates the boundary between the Hebridean Terrane and the Northern Highland Terrane (Fig. 1a). The MTZ was formed by large-scale horizontal shortening of the crust in the early Silurian which had largely ceased by c. 429 Ma (Goodenough et al., 2011). Archaean ('Lewisianoid') gneisses form the crustal basement of the Northern Highland Terrane (e.g., Friend et al., 2008; Moorhouse and Moorhouse, 1977) and similarities between mantle xenolith suites from the Hebridean and Northern Highland Terranes suggest that Archaean (Lewisian) lithospheric mantle also continues east beyond the MTZ (Hughes et al., 2015b). Hence the Lewisian underlies both terranes to the north of the GGF.

2.1.2. South of the GGF

In the Grampian Terrane, Palaeoproterozoic ('Rhinnian') gneisses are thought to be correlated with the Makkovikian–Ketilidian belt of Labrador and southern Greenland which borders the NAC to the south, see Fig. 1b (cf. Daly et al., 1991; Brown et al., 2003). This forms the basement to the late Proterozoic Dalradian supergroup and is inferred to extend from the Scottish west coast, eastwards for 600 km (e.g., Westbrook and Borradaile, 1978). Isotopic studies have established that the Rhinnian gneisses were derived from a depleted mantle source and represent comparatively juvenile crust with an age of c. 1.8 Ga. They are not considered to be a reworked or a southern extension of the NAC, but were instead part of an arc which underwent slab roll-back and extension before the break-up of Rodinia (Brown et al., 2003 and references therein). We note that the discovery of deep crustal Rhinnian gneiss xenoliths at Gribun (Upton et al., 1998) on the Isle of Mull (<20 km north of the GGF) indicates a lateral complexity in deep terrane boundaries (e.g., across the GGF).

Although the southern limit of the Rhinnian basement in the Grampian Terrane cannot be demonstrated, it has been suggested that it is truncated by the Highland Boundary Fault (cf., Pidgeon and Aftalion, 1978). Thus the southern margin of the Grampian Terrane is delineated by the Highland Boundary Fault (Fig. 1a). The Grampian event (after which the terrane is named) culminated in arc collision during which the Midland Valley Terrane became welded to the southern margin of the Grampian Terrane. The Southern Uplands Terrane is separated from the Midland Valley Terrane by the Southern Uplands Fault and the nature of the basement beneath it is still debated (see Oliver et al., 2008 and references therein). The Southern Uplands Terrane consists of a sequence of accretionary prisms (Leggett et al., 1979) that may involve both fore-arc and back-arc components (e.g., Stone et al., 1987). Mantle xenoliths from the Southern Uplands Terrane were not studied in the present investigation.

2.2. Mantle xenoliths

Virtually all mantle and deep crustal xenoliths and xenocrysts in Scotland were carried within Carboniferous and Permian minor alkali intrusions and diatremes that formed during a period of lithospheric extension north of the Variscan orogenic belt (Upton et al., 2004). This affected all five Scottish terranes to greater or lesser degrees. One exception is a small dyke at Loch Roag in the Hebridean Terrane that intruded in the mid-Eocene (47–46 Ma; Menzies et al., 1989; Faithfull et al., 2012). The host magmas range from basanites to silica-deficient compositions that the British Geological Survey sometimes refer to as monchiquites (mafic lamprophyre with brown amphibole, Ti-augite, olivine and biotite; see Gillespie and Styles, 1999). A general review of the xenolithic and megacryst-bearing localities was given by Upton et al. (1983) and Upton et al. (2011).

The localities containing upper mantle xenoliths span all five Scottish tectonic terranes (Fig. 1a). The majority of mantle xenoliths are spinel lherzolites (as used in this study), and whilst most of the associated pyroxenites are considered to be deep crustal cumulates, some are probably of sub-crustal derivation. A summary of the geology, geochemistry, petrology and alteration features of the studied peridotitic mantle xenoliths is provided in Table 1.

3. Sampling and analytical techniques

The map in Fig. 1a shows a selection of the xenolith localities included in this study. These include three localities to the north of the GGF; Loch Roag (LR), Streap Com'laidh (STP) and Rinibar (RNB), and four localities south of the GGF; Coire na Ba (CnC), Islay (ISL), Hillhouse (HH) and Patna (PNA). Additionally, we have included two xenolith suites from two different monchiquite dykes on the Isle of Colonsay (COL). Colonsay is regarded as a tectonic sliver within splays of the GGF and it is debatable to which terrane it ought to be ascribed (e.g., McAteer et al., 2010). The three northern localities were selected for the comparative freshness of their peridotite xenoliths, some of which are large enough to be used for both whole-rock and mineral analysis. By comparison, many xenolith suites in western Scotland south of the GGF included in this study have experienced carbonation, silicification and/or serpentinisation. Only samples from Patna and Hillhouse were large enough for bulk geochemistry whilst xenoliths from Coire na Ba, Islay and Colonsay were used for mineralogical studies only. All of the studied mantle xenoliths are spinel lherzolites.

3.1. Whole-rock sample preparation and analysis

Samples were provided by the British Geological Survey (Murchison House, Edinburgh) and the Hunterian Museum, University of Glasgow. Only xenoliths large enough for powdering were selected for whole-rock analysis but where material was limited, powdered samples weighed at least 25 g (typically 80–150 g for larger xenolith samples). The dykes hosting the xenoliths were also sampled for whole-rock analysis in order to compare their compositions with those of the xenoliths, and to assess whether dyke material remained during xenolith sample preparation.

Major and trace elements were analysed by inductively coupled plasma optical emission spectrometry (ICP-OES) and inductively coupled plasma mass spectrometry (ICP-MS), (see McDonald and Viljoen, 2006). Samples were analysed for PGE and Au by Ni sulphide fire assay followed by tellurium co-precipitation and ICP-MS (Huber et al., 2001; McDonald and Viljoen, 2006). Fire assay samples included multiple blanks and duplicate samples per assay batch, to assess any procedural contamination and nugget effect for smaller samples. Accuracy was constrained by analysis of certified reference materials TDB1, WMG1, WPR1, WITS1 and GP13 (for PGE + Au fire assay) and JB1a, NIM-P and NIM-N (for all other major and trace elements) — see Supplementary Material, Tables A and B. Precision was estimated by repeat analysis of a sub-set of samples (see Supplementary Material, Table C). Whole-rock analyses are presented in Table 2.

3.2. Petrography and mineral chemistry analysis

Xenolith textures were studied on polished thin sections and polished blocks, with mapping and quantitative microanalysis carried out on a Cambridge Instruments S360 scanning election microscope

Fig. 1. (a) Terrane map of Scotland, highlighting mantle xenolith localities (black dots). Suites used in this study are labelled accordingly: Loch Roag (LR), Streap Com'laidh (STP), Rinibar (RNB), Colonsay (COL), Islay (ISL), Coire na Ba (CnB), Hillhouse (HH) and Patna (PNA). These span four Terranes — the Hebridean Terrane, Northern Highland Terrane, Grampian Terrane and Midland Valley Terrane. (b) North Atlantic Craton and neighbouring orogenic belts in Greenland and Scotland, fragmented during the opening of the Atlantic Ocean. (For interpretation of the references to colour in this figure legend, the reader is referred to the web version of this article.)

Table 1
Overview table of xenolith suites used in this investigation.

Xenolith Suite	Terrane	Host dyke/sill	Thickness, strike/dip of host	Host dyke age	Xenoliths/Xenocryst suite	Mantle xenolith and xenocryst isotopic data	Peridotite texture(s) (Mercier & Nicolas, 1985)	Pervasive xenolith alternation/replacement (spinel lherzolites)	Melting textures in spinel lherzolites
Loch Roag	Hebridean	Monchiquite dyke	Approx. 70 cm wide, 075^{0}/ subvertical	45.2 Ma (Ar/Ar dating, Faithfull et al., 2012)	Lower crustal and mantle xenoliths (peridotites, pyroxenites, glimmerites, granulites, anorthosite, gabbros, syenites). Megacrysts (corundum/sapphires, feldspars, apatite, phlogophite)	$^{143}Nd/^{144}Nd$ 0.5118–0.5124, $^{87}Sr/^{86}Sr$ 0.7048–0.7051 (Upton et al., 2011), $^{206}Pb/^{204}Pb$ 17.139–17.348, $^{208}Pb/^{204}Pb$ 36.911–37.570 (Menzies et al., 1987), $^{187}Re/^{188}Os$ 1.411, $^{187}Re/^{188}Os_{intial}$ 0.0703 (Hughes et al., 2014)	Protogranular and porphyroclastic	No pervasive alteration. No alteration at xenolith 'cores' (low LOI/very minor serpentine). Xenolith rims (up to 1 cm thick) have abundant Fe-oxides and baryte.	Hercynite–feldspar symplectites, with outer zone of finer crystalline olivine and clinopyroxene.
Rinibar	Northern Highland (NE)	Alkali basalt dyke	Approx. 1 m wide dyke, striking NE-SW	252 ± 10 Ma (K/Ar age, Baxter & Mitchell, 1984)	Spinel lherzolites and pyroxenite megacrysts	$^{143}Nd/^{144}Nd$ 0.5124–0.5128, $^{87}Sr/^{86}Sr$ 0.7033–0.7038, $^{176}Hf/^{177}Hf$ 0.2828–0.2830 (CPX; Bonadiman et al., 2008). Fluid inclusions in olivine $^{3}He/^{4}He$ 2.84 ± 0.29, [^{4}He] 2.78 (Kirstein et al., 2004).	Protogranular and porphyroclastic	No pervasive alteration. Moderate serpeninitisation of olivine. Minor pockets of Ca-, Mg- and Fe-carbonate (interstitial to main silicate mineralogy of spinel lherzolite) in some xenoliths (e.g., sample E19). Carbonate-filled vugs are small (<300 μm wide) and occur mostly at olivine triple junctions.	A 200–500 μm wide zone along the xenolith margin lacks serpentinised fractures (which are otherwise abundant throughout the rest of the xenolith) - suggesting melting and reaction with the host monchiquite dyke. Olivine at the margin has recrystallised to olivine with a higher Si content than 'primary' olivine in the xenolith. 'Pockets' up to 500 μm diameter and irregularly shaped occur throughout xenoliths (core and margin). These consist of clinopyroxene, plagioclase, minor ilmenite (all <50 μm size crystals), skeletal chromite (<10 μm) and granular apatite (generally <10 μm), and are generally associated with carbonate (e.g., in sample E19).
Streap Com'laidh	Northern Highland (SW)	Monchiquite dyke	Approx. 70 cm, NE-SW trending/subvertical	c. 290 Ma (Walker & Ross, 1954; Upton et al., 2004)	Spinel lherzolites, websterites, pyroxenites, granulite-facies metagabbros and quartzo-feldspathic gneisses	$^{143}Nd/^{144}Nd$ 0.5121–0.5127, $^{87}Sr/^{86}Sr$ 0.7065–0.7083, $^{176}Hf/^{177}Hf$ 0.2825–0.2831 (Bonadiman et al., 2008). Fluid inclusions in olivine $^{3}He/^{4}He$ 6.01–6.33, [^{4}He] 9.26–63.3 (Kirstein et al., 2004).	Protogranular and porphyroclastic	None (low LOI/very minor serpentine). No pervasive alteration. However localised green and brown-coloured veinlets cross-cut some xenoliths (although timing of each set of veinlets is not clear). Green veins contain chlorite, baryte, calcite, clinopyroxene and plagioclase. Brown veins contain clinopyroxene, Ti-Fe-Mn oxide minerals and apatite.	Spinel-hercynite (mm-scale) is partially recrystallisation to higher Cr content (sometimes true chromite) dispersed as granular crystals (<20 μm). The spinel-chromite reaction rim is associated with plagioclase, minor grains of Fe-Ti(+/-Mn) oxides and some chlorite. Clinopyroxene can be observed with a high-Ca reaction rim in some xenoliths. In detail, clinopyroxene reaction rims consist of discrete granular crystals of higher-Ca clinopyroxene.
Colonsay	Grampian (at boundary with Northern	Two monchiquite dykes	no data available	Permo-Carboniferous(?) but not dated	Altered spinel lherzolites (in two separate dyke suites; 'CRB' and 'COD')	no data available	Generally protogranular (sometimes	Chlorite replacing highly/fully serpentinised olivine along crystal boundaries.	400 μm wide zone of xenolith melting at margins with host dyke. In immediate contact with

	Highland)						pervasively replaced)		the dyke is a dendritic zone of clinopyroxene intergrown with serpentine. Inward of this is a wider zone of fine granular and intergrown clinopyroxene and orthopyroxene (with chlorite) along with spinel-hercynite which has partially melted and disaggregated to chromite.
Islay	Grampian	Monchiquite dyke	no data available	Permo-Carboniferous(?) but not dated	Altered spinel lherzolites	no data available	Generally protogranular (sometimes pervasively replaced)	Complex and variable Ca- and Mg-carbonate and quartz replacement textures (i.e., pervasive alteration is present).	Minor disaggregation at margins of clinopyroxene.
Coire na Ba	Grampian	Monchiquite dyke	no data available	Permo-Carboniferous(?) but not dated	Altered spinel lherzolites	no data available	Generally protogranular (sometimes pervasively replaced)	Complex serpentine (and chlorite) - quartz replacement textures (i.e., pervasive alteration is present).	Spinel crystals can have extensive reaction rims to chromite. Clinopyroxene crystals sometimes preserve a reaction rim of skeletal or dentritic low-Cr clinopyroxene intergrown with plagioclase (albite). Dendrites (in a zone approximately 100 μm wide) abutt a rounded zone (approximately 300 μm wide) of graphic melting between fine (<25 μm) orthopyroxene and clinopyroxene.
Hillhouse	Midland Valley	Olivine dolerite sill	>20 m thick	Permo-Carboniferous but not dated	Fresh spinel lherzolites (only)	no data available	Generally protogranular	Very minor serpentine. No pervasive alteration.	Melt pockets of finely crystalline (10–30 μm) symplectites of clinopyroxene and olivine, surrounded by coarse un-melted silicates (mostly olivine and orthopyroxene). Melting has been restricted to clinopyroxene-olivine contact zones. Minor partially recrystallised higher-Cr rims to spinel crystals also noted.
Patna	Midland Valley	Volcanic breccia (contacts not seen)	>100 m, unknown strike / assumed vertical	Permian(?) but not dated	Altered spinel lherzolites	no data available	Protogranular (pervasively replaced)	Pervasively replaced by Ca-carbonate (zoned in Mn and Fe) and quartz, with relict orthopyroxene now mostly replaced by serpentine. Replacement minerals have preserved the original protogranular texture of the xenolith silicate mineralogy.	n/a (pervasive carbonate and quartz alteration does not show evidence of relic melting textures). Rare relic olivine and clinopyroxene, some spinel.

Table 2
Bulk rock geochemistry for xenoliths and host dykes. Note that for Loch Roag samples marked with *, bulk rock data has already been published in Hughes et al. (2014). For whole-rock analyses this included seven separate xenoliths of approximately 3–6 cm diameter from Loch Roag (see Hughes et al., 2015b and Hughes, 2015 for further details), two larger angular xenoliths (10–20 cm) from Rinibar, five large xenoliths (ranging 10–15 cm diameter) from Streap Com'laidh, three carbonated xenoliths from Patna (ranging 5–15 cm diameter) and four fresh xenoliths from Hillhouse (2–5 cm).

Sample number	Suite	Lithology	SiO_2	Al_2O_3	Fe_2O_3	MgO	CaO	Na_2O	K_2O	TiO_2	MnO	P_2O_5	LOI	Total	Mg#	Sc	V	Cr	Co	Ni	Cu	Rb	Sr	Y	Zr	Nb
Xenoliths			*(wt.%)*													*(ppm)*										
LR81*	Loch Roag	Spinel lherzolite	45.34	2.40	10.12	35.78	2.54	0.46	0.54	0.03	0.16	0.15	3.25	100.78	0.89	13.47	60.14	2910	107.4	1756	98.3	5.53	255.6	6.93	4.56	0.37
LR101335*	Loch Roag	Spinel lherzolite	42.85	1.06	11.48	38.16	2.61	0.16	0.03	0.05	0.25	0.22	2.37	99.23	0.88	9.22	36.56	2599	130.0	2404	69.7	1.19	93.6	9.67	16.41	3.42
LR289*	Loch Roag	Spinel lherzolite	43.97	1.89	10.05	37.04	2.53	0.30	0.11	0.06	0.17	0.12	3.29	99.53	0.89	11.65	48.21	3001	132.6	2022	97.0	2.73	250.5	9.42	6.53	0.98
LR80*	Loch Roag	Spinel lherzolite	45.33	1.59	10.20	38.71	2.22	0.44	0.09	0.03	0.13	0.04	0.92	99.70	0.90	12.04	47.35	2456	103.1	2144	182.2	2.27	28.2	4.36	5.70	1.12
E19	Rinibar	Spinel lherzolite	42.34	1.46	7.86	32.90	2.30	0.21	0.07	0.07	0.11	0.07	11.92	99.30	0.91	10.00	44.30	2212	98.9	2040	66.8	2.76	148.1	2.24	4.85	3.16
G8R2xnl	Rinibar	Spinel lherzolite	42.03	2.37	8.59	34.01	3.81	0.28	0.07	0.16	0.15	0.02	7.73	99.22	0.91	11.24	55.04	2454	90.7	1663	26.9	2.63	209.1	3.47	30.96	5.70
2	Streap Com'laidh	Spinel lherzolite	45.77	3.16	9.11	36.82	2.77	0.26	0.03	0.14	0.12	0.01	1.61	99.81	0.91	14.74	56.54	2274	87.8	2038	41.4	0.96	26.1	3.22	5.35	1.83
5	Streap Com'laidh	Spinel lherzolite	47.56	3.37	8.96	34.44	3.46	0.29	0.01	0.15	0.12	0.02	1.20	99.58	0.90	13.48	69.38	3167	98.6	1882	136.6	0.85	45.8	3.67	6.58	1.43
4b	Streap Com'laidh	Spinel lherzolite	46.85	3.42	9.75	35.59	2.75	0.26	0.06	0.12	0.13	0.01	2.31	101.24	0.90	13.11	59.91	2399	95.3	2227	74.0	2.09	37.5	2.95	3.38	1.90
4a	Streap Com'laidh	Spinel lherzolite	43.96	3.11	9.84	37.12	2.71	0.21	0.04	0.12	0.13	0.02	2.61	99.87	0.90	13.38	57.88	2656	100.4	2380	57.8	1.36	101.5	3.01	5.12	2.18
4c	Streap Com'laidh	Spinel lherzolite	47.53	3.19	9.51	34.43	2.89	0.29	0.05	0.13	0.13	0.02	0.96	99.13	0.90	13.89	58.91	2531	96.1	2127	153.2	1.24	54.4	3.00	3.99	1.82
63	Patna	Spinel lherzolite	48.40	3.08	3.13	4.18	22.67	0.01	0.05	0.12	0.27	0.02	19.17	101.10	0.82	14.11	62.80	4443	149.5	840	253.1	1.45	205.2	7.76	35.26	3.16
64	Patna	Spinel lherzolite	32.93	1.36	2.57	3.67	33.17	0.06	0.08	0.12	1.00	0.05	25.89	100.88	0.84	15.01	55.51	5238	217.8	1164	175.0	2.28	381.2	6.88	21.82	3.73
62	Patna	Spinel lherzolite	36.97	3.06	3.85	7.02	26.14	0.16	0.02	0.07	0.61	0.01	22.80	100.72	0.84	19.02	82.72	4164	229.7	1258	93.4	0.47	210.2	6.90	5.66	1.48
HHX1xnl	Hillhouse	Spinel lherzolite	44.84	3.30	8.13	37.00	2.97	0.34	0.16	0.13	0.13	0.02	2.32	99.33	0.92	13.01	63.41	2640	94.5	1774	25.3	6.64	19.2	2.78	6.26	1.25
HHX4xnl	Hillhouse	Spinel lherzolite	44.54	3.49	9.38	36.13	2.73	0.38	0.25	0.18	0.15	0.03	3.41	100.66	0.90	11.52	60.98	2272	98.4	1775	95.7	7.32	33.8	3.42	11.35	1.71
HHX2xnl	Hillhouse	Spinel lherzolite	42.58	3.77	8.99	36.52	2.02	0.26	0.16	0.15	0.14	0.02	4.38	99.00	0.91	10.74	56.51	2538	100.2	1783	42.7	3.76	15.9	2.26	4.83	0.47
HHX3xnl	Hillhouse	Spinel lherzolite	46.36	1.16	7.62	40.68	0.85	0.25	0.21	0.07	0.13	0.04	2.31	99.68	0.93	6.88	32.59	2870	94.5	2001	15.6	6.37	88.3	2.15	10.96	2.49
Host dykes																										
LRh	Loch Roag	Monchiquite	44.88	14.85	8.48	7.75	10.84	1.91	3.49	2.73	0.21	1.19	4.65	100.95	0.78	21.80	212.68	230	36.3	136	51.6	39.88	1797.0	28.03	346.82	100.76
HHX4dyke	Hillhouse	Olivine dolerite	45.10	14.60	12.17	11.30	10.37	2.57	1.01	1.87	0.20	0.31	1.81	101.31	0.72	28.71	235.44	484	55.1	2644	182.0	28.75	438.7	20.91	102.83	28.00
HHX1dyke	Hillhouse	Olivine dolerite	45.19	14.97	11.10	11.42	10.83	2.68	1.11	1.70	0.20	0.36	1.41	100.98	0.74	28.11	235.10	469	53.9	258	68.8	31.01	449.7	21.37	120.45	29.74
R2dyke	Rinibar	Lamprophyre	38.51	9.56	10.33	20.36	8.48	0.79	0.81	1.91	0.22	0.74	8.30	100.01	0.85	21.83	185.39	944	58.9	568	75.0	34.73	392.9	22.23	120.21	72.80
P1	Patna	Volcanic breccia plug	52.85	11.01	8.44	8.75	5.74	1.57	1.53	1.19	0.14	0.39	8.49	100.11	0.75	14.42	131.32	944	35.6	2766	49.2	38.83	283.8	21.37	206.14	39.65

Table 2 (*continued*)

Sample number	Ba	La	Ce	Pr	Nd	Sm	Eu	Gd	Tb	Dy	Ho	Er	Tm	Yb	Lu	Hf	Ta	Th	U	Os	Ir	Ru	Rh	Pt	Pd	Au	Total PGE + Au	Co/Ni
Xenoliths																				*(ppb)*								
LR81*	47.8	100.23	216.44	15.96	40.74	4.36	0.75	3.59	0.33	1.39	0.22	0.64	0.09	0.54	0.08	0.14	0.02	2.71	0.73	2.75	3.08	5.79	1.35	12.52	6.35	2.28	34.10	0.06
LR101335*	25.8	54.65	135.63	12.26	35.78	4.72	0.93	3.78	0.41	2.00	0.32	0.89	0.13	0.78	0.11	0.42	0.19	0.89	0.24	3.29	3.48	5.77	1.54	11.69	5.00	2.00	32.77	0.05
LR289*	37.6	87.14	213.27	20.02	53.41	6.47	1.12	4.80	0.47	2.11	0.34	0.97	0.14	0.87	0.13	0.17	0.06	2.81	1.02	3.63	3.64	6.41	1.68	11.07	4.70	3.30	34.44	0.07
LR80*	13.2	18.91	21.13	2.74	7.89	0.93	0.22	0.82	0.10	0.58	0.11	0.32	0.05	0.32	0.05	0.14	0.07	1.26	0.33	3.45	3.60	6.03	1.47	16.88	11.48	1.96	44.86	0.05
E19	63.9	10.45	17.57	2.00	6.90	1.06	0.27	0.82	0.09	0.41	0.08	0.24	0.04	0.19	0.03	0.09	0.17	0.82	0.22	1.92	3.04	6.02	1.03	6.59	4.81	2.11	25.52	0.05
G8R2xnl	78.1	10.09	15.73	1.68	5.87	1.02	0.32	0.95	0.13	0.65	0.12	0.34	0.05	0.31	0.06	0.77	0.34	1.37	0.41	3.07	2.99	5.89	0.86	5.23	3.55	0.64	22.22	0.05
2	8.3	0.50	1.07	0.16	0.84	0.27	0.11	0.32	0.07	0.48	0.10	0.31	0.05	0.33	0.06	0.09	0.10	0.27	0.06	2.94	2.99	5.73	1.00	7.40	3.98	1.95	26.00	0.04
5	2.7	1.06	2.32	0.31	1.38	0.39	0.13	0.39	0.07	0.55	0.11	0.34	0.05	0.34	0.06	0.17	0.08	0.29	0.07	2.76	3.32	6.41	1.16	8.04	6.16	2.57	30.42	0.05
4b	14.6	1.26	2.24	0.28	1.16	0.29	0.11	0.31	0.06	0.44	0.09	0.28	0.05	0.30	0.05	0.08	0.11	0.41	0.09	0.43	0.55	1.61	0.31	1.39	1.38	1.48	7.13	0.04
4a	9.4	1.31	2.41	0.30	1.29	0.33	0.11	0.35	0.06	0.46	0.09	0.28	0.04	0.28	0.05	0.11	0.11	0.40	0.09	2.89	4.83	6.54	1.96	8.23	6.46	14.47	45.37	0.04
4c	8.3	1.08	2.18	0.29	1.25	0.32	0.11	0.31	0.06	0.47	0.09	0.27	0.04	0.31	0.05	0.10	0.11	0.34	0.12	2.97	3.74	6.83	1.32	6.50	5.67	2.88	29.90	0.05
63	28.0	29.81	50.59	5.89	22.37	3.72	0.94	2.92	0.33	1.35	0.19	0.49	0.05	0.36	0.06	0.59	0.15	0.55	0.12	3.80	4.10	8.76	1.47	9.55	7.68	2.17	37.52	0.18
64	82.0	22.14	40.62	4.57	16.37	2.14	0.61	1.97	0.22	1.01	0.16	0.45	0.06	0.33	0.06	0.41	0.18	0.92	0.25	4.99	5.40	9.42	1.39	7.01	2.41	1.43	32.05	0.19
62	11.0	13.71	29.76	4.05	16.20	2.10	0.51	1.87	0.21	0.98	0.16	0.46	0.06	0.37	0.06	0.11	0.08	0.25	0.07	4.63	5.36	10.27	1.80	9.99	7.34	2.81	42.20	0.18
HHX1xnl	26.4	0.64	1.53	0.21	0.90	0.29	0.10	0.33	0.06	0.42	0.10	0.31	0.05	0.32	0.05	0.15	0.08	0.17	0.04	0.87	0.85	1.50	0.31	1.49	1.14	0.23	6.38	0.05
HHX4xnl	35.6	1.45	3.33	0.45	2.00	0.49	0.16	0.52	0.09	0.55	0.12	0.37	0.06	0.36	0.06	0.25	0.09	0.27	0.12	1.79	3.30	6.22	1.28	7.59	5.91	1.08	27.17	0.06
HHX2xnl	13.8	0.34	1.08	0.17	0.86	0.26	0.09	0.28	0.05	0.39	0.08	0.26	0.04	0.28	0.05	0.11	0.03	0.10	0.06	2.96	2.89	6.57	1.17	6.71	5.20	1.48	26.97	0.06
HHX3xnl	61.3	5.91	11.15	1.34	4.82	0.85	0.23	0.64	0.08	0.42	0.08	0.21	0.03	0.17	0.02	0.19	0.15	0.59	0.15	5.19	4.77	9.44	1.47	5.29	1.67	1.27	29.10	0.05
Host dykes																												
LRh	2557.7	132.11	239.79	27.04	91.41	12.87	3.65	10.72	1.24	5.48	0.95	2.55	0.34	2.06	0.31	8.42	4.97	8.59	2.56	0.02	0.05	0.15	0.05	0.68	0.44	0.05	1.44	0.27
HHX4dyke	460.1	18.46	38.86	5.07	21.33	4.52	1.51	4.58	0.72	3.72	0.69	1.91	0.28	1.73	0.26	2.54	1.52	2.57	0.70	0.04	0.04	0.21	0.06	0.75	0.40	0.16	1.66	0.02
HHX1dyke	440.6	19.20	39.82	5.27	21.58	4.65	1.49	4.64	0.70	3.68	0.72	2.01	0.28	1.72	0.27	3.01	1.53	2.23	0.74	0.12	0.08	0.17	0.10	2.08	0.64	0.60	3.77	0.21
R2dyke	648.8	52.00	92.65	10.90	40.14	7.32	2.18	6.79	0.90	4.27	0.74	1.97	0.26	1.54	0.25	3.08	3.85	6.35	2.03	-	-	-	-	-	-	-	-	0.10
P1	560.5	33.30	63.79	7.82	28.81	5.36	1.51	4.99	0.74	3.67	0.69	1.90	0.27	1.72	0.27	5.05	1.97	5.96	1.51	0.27	0.25	0.58	0.17	1.04	0.65	0.51	3.46	0.01

Table 3
Calculated modal abundances (by % area per whole thin section scan) of sulphides for selected xenoliths and xenolith suites. See main text for methodology and Supplementary PNG files of false colour phase maps of the corresponding sample thin sections.

Sample number	Suite	Lithology	Modal % (area) sulphide
LR80-1	Loch Roag	Spinel lherzolite	0.072
LR80-2	Loch Roag	Spinel lherzolite	0.096
LR80-3	Loch Roag	Spinel lherzolite	0.185
LR90	Loch Roag	Spinel lherzolite	0.035
E19	Rinibar	Spinel lherzolite	0.103
CRB-39	Colonsay	Spinel lherzolite	0.048
COD-4	Colonsay	Spinel lherzolite	0.106

(SEM) at Cardiff University. Quantitative microanalyses were obtained using an Oxford Instruments INCA Energy EDS analyser attached to the SEM, with operating conditions set at 20 kV and specimen calibration current of ~2 nA at a fixed working distance of 25 mm. Analytical drift checks were carried out every 2 hours using the Co reference standard and a comprehensive suite of standards from MicroAnalysis Consultants Ltd were used to calibrate the EDS analyser.

Polished thin sections, and some corresponding polished blocks for samples requiring sulphide trace element analysis were selected for laser ablation ICP-MS (LA-ICP-MS). LA-ICP-MS was performed on sulphide minerals at Cardiff University. Both line and spot analyses were used and independently calibrated, depending on the size of the sulphides. For lines, a minimum line length of ~80 μm and a beam diameter of 15 μm was used, with laser operating conditions of 10Hz frequency, generating ~5 J cm^{-2} energy and sample translation at 6 μm s^{-1}. For spot analysis, beam size was 40 μm with the same laser operating conditions. Individual sulphide minerals (or mineral clusters) < 80 μm across were analysed by spot analysis. Acquisition times ranged from 40 to 180 s with a gas blank measured for 30–40 s prior to laser ablation.

Major element concentrations were measured prior to LA-ICP-MS on the SEM, and ^{33}S was used as an internal standard for trace element calibration. Gas blank subtraction and internal standard corrections were carried out on Thermo Plasmalab software. Synthetic Ni-Fe-S quenched sulphide standards were used for LA-ICP-MS machine calibration, including S, Ni, Fe and Cu as major elements, and Co, Zn, As, Se, Ru, Rh, Pd, Ag, Cd, Sb, Te, Re, Os, Ir, Pt, Au and Bi as trace elements. The compositions and details of analysis methods for these standards are presented in the supplementary material of Prichard et al. (2013) and further procedural details are available in Smith et al. (2014). Standards 1, 2 and 3 were used for calibration of Fe, Ni, Cu, Co and Zn, as well as matrix-matched corrections for argide species which interfere with light PGE isotopes ($^{59}Co^{40}Ar$, $^{61}Ni^{40}Ar$, $^{63}Cu^{40}Ar$, $^{65}Cu^{40}Ar$ and $^{66}Zn^{40}Ar$). Standard 1 was also used in corrections for ^{106}Cd on ^{106}Pd and ^{108}Cd on ^{108}Pd. Argide and isobaric-corrected data are presented in Table E (Supplementary Material) for Ru, Rh and Pd. Independent corrections for various isotopes of the same element (e.g., $^{66}Zn^{40}Ar$ and ^{106}Cd on ^{106}Pd, and ^{108}Cd on ^{108}Pd)

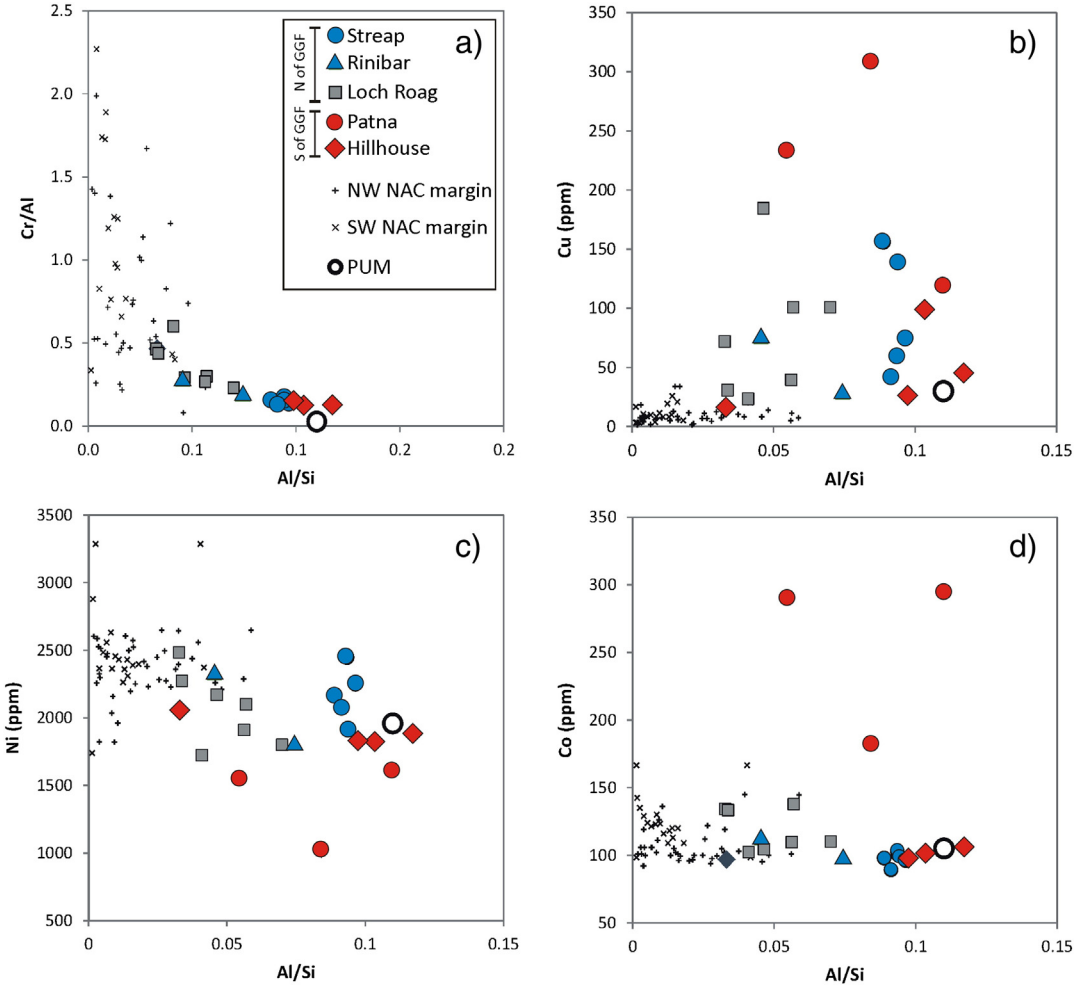

Fig. 2. Bulk rock geochemistry (a) Major element ratios; (b) Cu *vs.* Al/Si; (c) Ni *vs.* Al/Si; (d) Co *vs.* Al/Si. Note that Patna xenoliths are highly carbonated and plots displayed are for anhydrous data corrected by LOI (so all bulk rock data is plotted for anhydrous compositions). NW and SW NAC margin xenoliths are from Wittig et al. (2010). Primitive Upper Mantle (PUM) is from McDonough and Sun (1995).

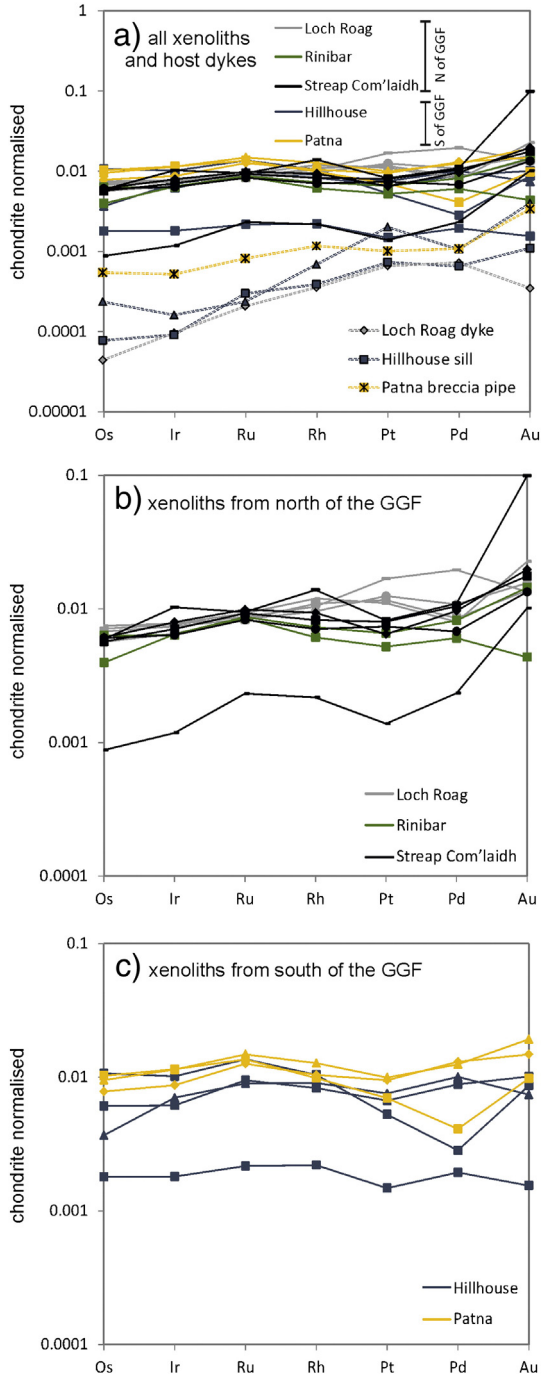

Fig. 3. Bulk rock platinum-group element multi-element diagrams, chondrite-normalised (McDonough and Sun, 1995) and according to xenolith suite; (a) all xenoliths and host dykes, sills and vents which entrained the xenoliths; (b) xenoliths from north of the Great Glen Fault; (c) Xenoliths from south of the Great Glen Fault.

showed < 20% (commonly < 5%) variance, indicating that the correction criteria are suitable. Accuracy for PGE and Au was checked by analysis of the standard Laflamme-Po724 as an unknown against the Cardiff quenched sulphide standards (results in Supplementary Material Table F). The small size of many sulphides prevented repeat analyses and 1σ precision based on TRA counting statistics are typically 2–16% (concentrations 10–100 ppm), 10–27% (1–10 ppm) and 23–80% (<1 ppm). A representative selection of time resolved analysis spectra (TRA) for sulphide minerals analysed are presented in the Supplementary Material and all LA-ICP-MS data are in Supplementary Table E.

3.2.1. Element maps and modal abundances of sulphide

Whole thin-section element maps of the samples were collected on a Zeiss Sigma HD analytical SEM outfitted with dual 150 mm^2 active area EDS detectors at Cardiff University. Using a 20 μm step-size and a pixel dwell time of 15 ms, EDS analyses create effective phase maps for pyroxenes, olivine, spinel, feldspars, sulphides, carbonates and phosphates (see Supplementary Material for all images and maps — PNG files named 'LR80-' and 'LR90-' accordingly). The modal abundance of sulphide minerals (counted as total sulphide without differentiating between Ni, Fe, or Cu end-member compositions) was estimated in each case using the built-in PhaseMap tool in Oxford Instruments Aztec Energy software, which accounts for the shape and/or boundaries of xenolith(s) within one thin section. The modal abundances of sulphide for each scanned thin section are provided in a Table 3 which accompanies the phase maps in the Supplementary Material.

4. Results

4.1. Xenolith preservation and alteration

Xenolith textures (e.g., protogranular and porphyroclastic) are summarised in Table 1 and a selection of whole thin section modal maps are shown in the Supplementary PNG files demonstrating the texture of most xenolith suites. Xenoliths from suites north of the GGF generally retain their primary silicate mineralogy (olivine, orthopyroxene, clinopyroxene and spinel). In some cases alteration around the margins of xenoliths (restricted to the outermost 5–10 mm) is recorded as overprinting by baryte and Fe-oxides (e.g., Loch Roag — Table 1). Xenoliths from Rinibar are moderately serpentinised, as reflected in their elevated LOI (Table 2). Despite fracturing, primary silicate chemistry is preserved (see Upton et al., 2011 and references therein). Olivine is partially replaced by serpentine. Small 'pockets' (<300 μm wide) of Ca-, Mg- and Fe-carbonates occur interstitially to the primary silicates and can contain sulphide minerals (see Section 4.3).

The xenoliths from south of the GGF are typically altered such that little fresh olivine and/or orthopyroxene remain (see Table 1 for details). However, the alteration products are not consistent from one suite to another. For example, whilst carbonate replacement is commonplace in Patna and Islay xenoliths, this varies from Ca-carbonate (zoned in Mn and Fe) at Patna, to both Ca- and Mg-carbonates at Islay. Quartz replacement is present in some Patna, Islay and Colonsay xenoliths, and can be coupled with carbonate and/or serpentine replacement also. The original mineralogy of peridotite xenoliths is locally preserved as patches of silicates that have been resistant to replacement (for example relic olivine in Colonsay xenoliths). In most cases, pervasive alteration has nonetheless retained patches of the original silicate mineral textures allowing petrography, particularly of interstitial sulphides, to be discerned. We highlight that this pervasive alteration in xenoliths from south of the GGF is distinct from carbonate found in xenoliths from north of the GGF (e.g., Rinibar) in which primary peridotitic mineralogy is retained and the carbonates are strictly as small, rare interstitial melt 'pockets'. Hillhouse xenoliths are the exception for southern xenolith suites, as these are fresh peridotites with unaltered silicate mineralogy (except for very minor serpentinisation of olivine) and lack pervasive alteration of the type(s) described above. The textural relationships of sulphide minerals are outlined in Section 4.3 and Supplementary Table D.

4.2. Whole-rock element abundances

4.2.1. Major elements and Ni, Cu and Co

Cr/Al and Al/Si ratios are used as a proxy for the degree of depletion in Fig. 2a. Mantle xenoliths (harzburgites, lherzolites and wehrlites) from the North Atlantic Craton (NAC) in west Greenland have low Al/Si and

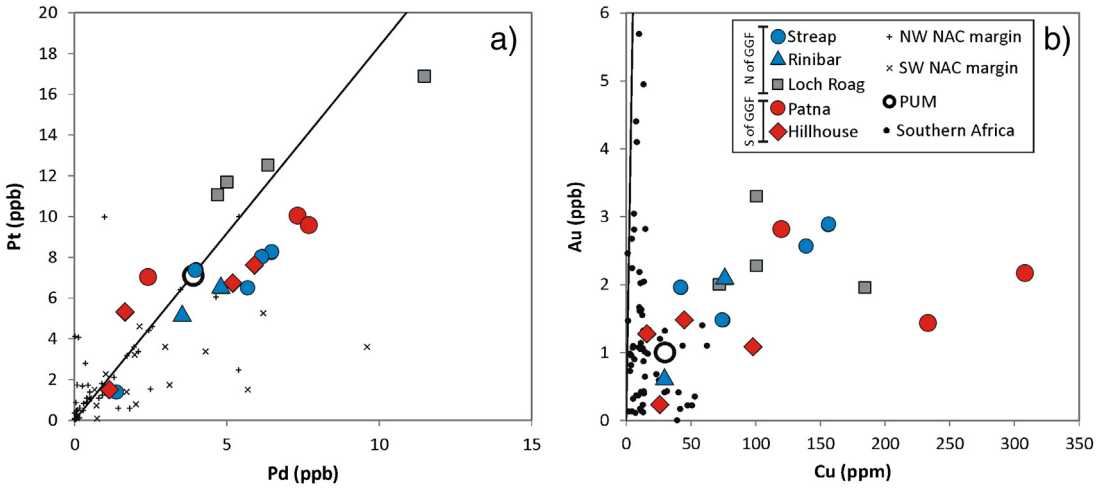

Fig. 4. Bulk rock binary diagrams for Pt *vs.* Pd (a) and Au *vs.* Cu (b). NW and SW NAC margin xenoliths are from Wittig et al. (2010). Southern African data from Maier et al. (2012). Primitive Upper Mantle (PUM) is from McDonough and Sun (1995). Black line indicates chondritic ratio of elements (McDonough and Sun, 1995).

extremely variable Cr/Al (Wittig et al., 2010) relative to 'Primitive Upper Mantle' (PUM; McDonough and Sun, 1995). Loch Roag and Rinibar xenoliths overlap these compositions — although harzburgites are absent. By comparison, the Streap Com'laidh and Hillhouse xenoliths more closely resemble the PUM. Due to the extensive carbonation of Patna xenoliths, these could not be plotted in Fig. 2a.

Anhydrous Cu and Ni concentrations are plotted versus Al/Si (anhydrous) as a proxy for depletion (Fig. 2b–c). This highlights a significant enrichment in Cu for all the Scottish xenoliths (Fig. 2b). In particular, the Patna xenoliths have extremely elevated Cu but this is in part an artefact of the anhydrous correction (which is particularly high for these xenoliths due to the abundance of carbonate, also manifest in the very low MgO). 'Raw' (i.e., not LOI corrected) maximum Cu abundance is 253 ppm (see Table 2) and hence, Cu abundance in Patna is within range of the other (fresh and not pervasively altered) Scottish xenoliths from north of the GGF. Ni and Co contents of Loch Roag, Rinibar, Streap Com'laidh and Hillhouse xenoliths (Fig. 2c–d) are within range of the Greenland NAC xenoliths and PUM. The Patna xenoliths (for reasons pertaining to the anhydrous correction) appear to have lower Ni contents. However, for 'raw' Co abundances, the Patna xenoliths are notably enriched and have Co/Ni ratios > 0.1, unlike other xenoliths which have Co/Ni < 0.1 (see Table 2). This enrichment cannot be ascribed to carbonation or to the anhydrous (LOI-based) correction.

4.2.2. Platinum-group elements and gold

All the xenoliths are enriched by one or more orders of magnitude above the composition of their dyke hosts, and fractionation between Ir-group platinum-group elements (IPGE) and Pd-group platinum-group elements (PPGE) is notably different, confirming that PGE contamination from the host magmas was insignificant (Fig. 3a).

Broadly, the chondrite-normalised IPGE patterns for the spinel lherzolite xenoliths form a cluster from ~0.002 to 0.010 × chondrite and are essentially flat (Fig. 3a). IPGE abundances for xenoliths from north of the GGF are tightly clustered in comparison to PPGE patterns (Fig. 3b) or xenoliths from south of the GGF (Fig. 3c). The Streap Com'laidh spinel lherzolites display systematic positive anomalies for Au (but are not actually enriched in Au in terms of raw ppb abundance) due to a slight negative anomaly for Pt. One of the Streap Com'laidh xenoliths has a PGE pattern with notably lower normalised abundances (displaced by one order of magnitude). Duplicates show that this lower PGE abundance is a consistent feature of the xenolith sample, and it could indicate a lower modal abundance of PGE-bearing (sulphide) phases in this particular sample.

Most strikingly, the Loch Roag xenoliths always have elevated Pt in comparison to all other xenolith suites (Fig.3b) whereas Pt is always slightly depleted relative to Rh and IPGE in the other xenolith suites. A binary plot of Pt *vs.* Pd in Scottish and Greenlandic NAC xenoliths (Wittig et al., 2010) is presented in Fig. 4a. Whole-rock Pt *vs.* Pd trends (Fig. 4a) for the Scottish xenoliths mainly fall along a linear trend (approximating chondritic ratios) whereas most of the Greenlandic NAC xenoliths have lower absolute Pt + Pd concentrations than PUM and Pt/Pd ratios lower than chondrite.

Since no published data for the concentration of Au in the Greenlandic NAC xenoliths are available we compare the Scottish Au contents with those of Southern African cratonic xenoliths (Maier et al., 2012; Fig. 4b). Au and Cu in the fresh Scottish xenoliths (i.e., from north of the GGF) display a broad positive correlation, in contrast to the Southern African xenoliths where the Au concentrations show no correlation with Cu. For the pervasively altered Patna xenoliths, there is no correlation between Cu and Au.

4.3. Sulphide petrography and mineralogy

Comprehensive descriptions of the mineralogy, textures and general petrography of sulphide minerals in the Scottish peridotite xenoliths are given in Supplementary Table D (which refers to textural classifications in Fig. 5) and Table 3 provides the modal percentage of sulphide that has been calculated from whole thin-section scans (by SEM). The majority of sulphides are interstitial to the silicates and consist of mixtures of base metal sulphide minerals (pentlandite, pyrrhotite and chalcopyrite). A systematic scheme for categorising sulphide minerals according to the number of sulphide phases, morphology, textures, and replacements/alteration, has been adopted in order to ensure clarity and consistency of descriptive terms herein. This scheme is broadly founded upon ore textures in Craig and Vaughan (1994) and describes features laid out in Fig. 5. Whilst this scheme is not exhaustive it incorporates all the textures so far encountered in the Scottish xenoliths.

4.3.1. North of the GGF

Two 'populations' of mixed base metal sulphides have been identified in the Loch Roag lherzolite xenoliths. These have been ascribed to different populations due to their distinct textures and petrography (Fig. 6). A detailed discussion of the petrography of these co-existing sulphide populations is provided in Hughes (2015) and we give an overview of the most salient points here: (a) One group of mixed base metal sulphides are coarse, interstitial to the silicates and irregularly shaped with complex textures (from herein these are referred to as 'Loch Roag complex sulphides'; Fig. 6a). (b) By contrast, a second group of

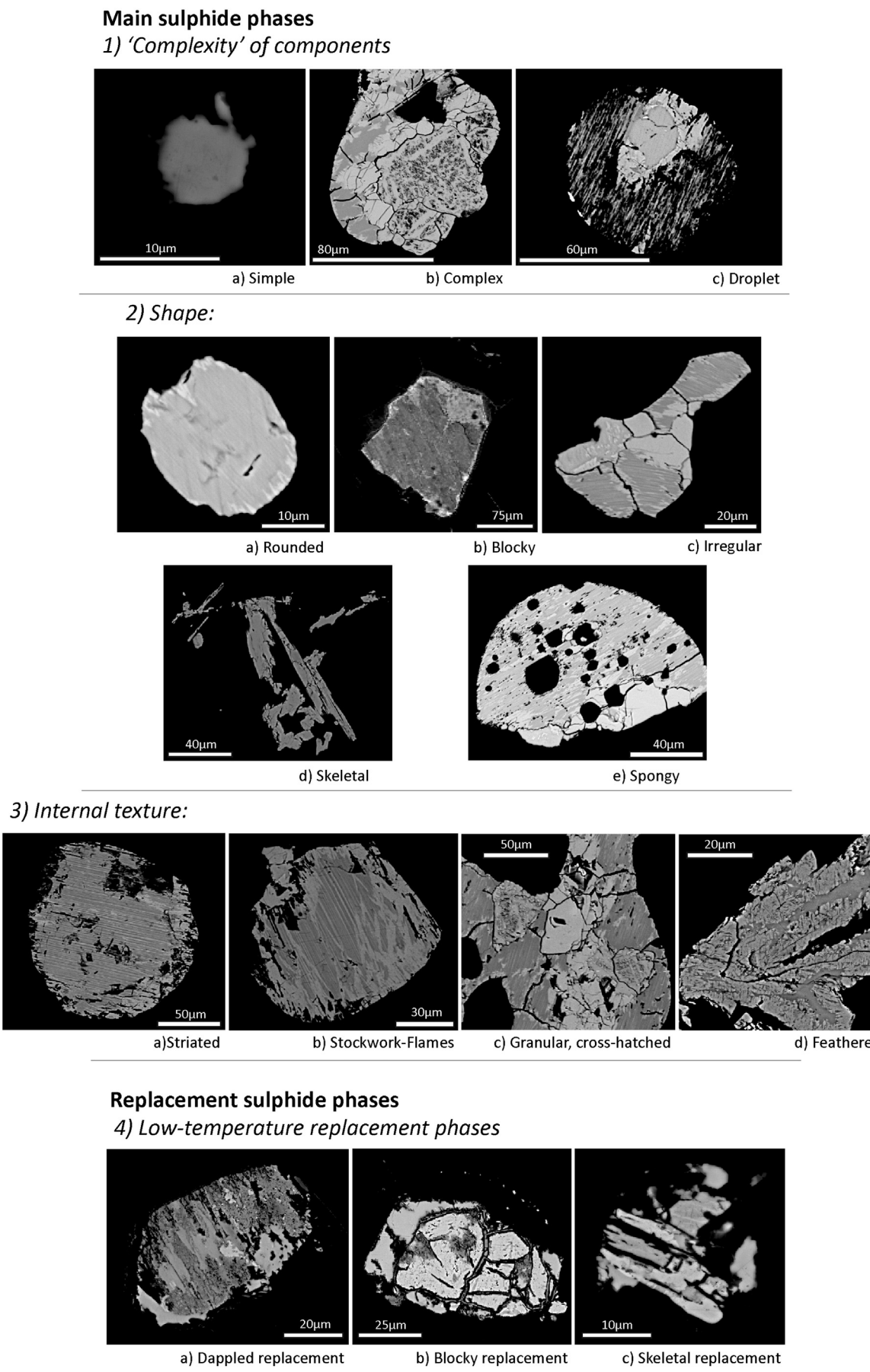

Fig. 5. Classification categories for sulphide petrography and textures (refers to Supplementary Table D).

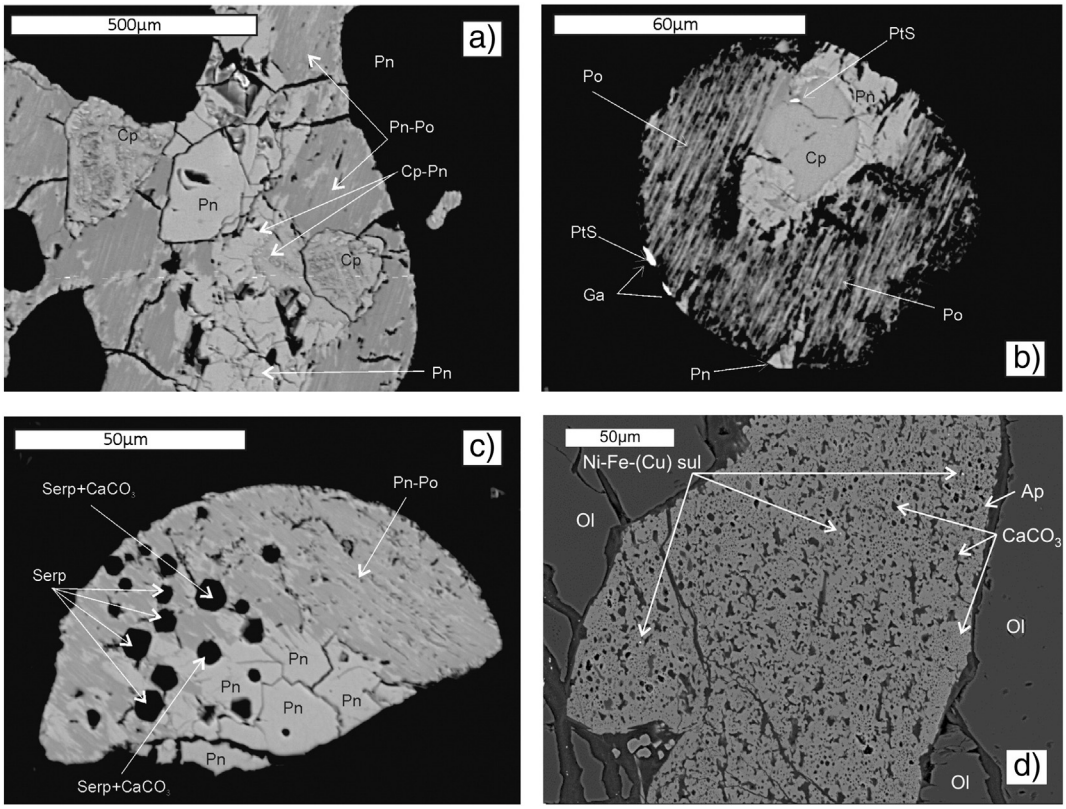

Fig. 6. Loch Roag xenolith SEM backscatter electron images (BSE). (a) Irregular-shaped 'complex sulphide' with granular pentlandite and cross-hatched chalcopyrite which are texturally distinct from the surrounding pentlandite, pentlandite–pyrrhotite stockwork, and striated pyrrhotite. (b) Rounded 'droplet sulphide' showing pentlandite and chalcopyrite have separated from striated pyrrhotite (with minor pentlandite flames). Discrete µm-scale platinum-group minerals occur within this high-PGE sulphide droplet. Pt-sulphide (probably cooperite) is within chalcopyrite portion and at the margin of the droplet. Pt-sulphide at the droplet margin occurs with galena. (c) Spongey 'droplet sulphide' with partially serpentinised and Ca-carbonate filled inclusions. (d) Spongey apatite between olivine crystals. Note that the sponey texture is due to abundant rounded Ca-carbonate inclusions (dull 'holes' in apatite) as well as minor rounded Ni-Fe-(Cu) sulphide droplets as inclusions (bright spots). Mineral abbreviations are: olivine (Ol), serpentine (Serp), apatite (Ap), pentlandite (Pn), chalcopyrite (Cp), pyrrhotite (Po), cooperite (PtS), galena (Ga), Ca-carbonate ($CaCO_3$).

mixed base metal sulphides (co-existing with the former group in the same xenoliths) are rounded droplets (Fig. 6b), sometimes spongey in appearance due to the presence of rounded Ca-carbonate inclusions (Fig. 6c). These droplets (herein referred to as 'Loch Roag droplet sulphides') strictly occur within spinel-feldspar symplectites which run through the xenoliths. The droplet sulphides often bear discrete micron-scale PtS (cooperite) — Hughes et al. (2014). We also note that apatite crystals up to 300 µm in length occur in Loch Roag xenoliths. Apatites are commonly also spongey, with abundant rounded inclusions of Ca-carbonate and micron-sized droplets of Ni-Fe-(Cu) sulphide (Fig. 6d).

Two groups of base metal sulphides occur in the Rinibar xenolith suite. These groups are defined according to the relative abundance of chalcopyrite *vs.* Ni-Fe sulphides, and the types of minerals surrounding the sulphides. For example, sample R2 has a low abundance of carbonate minerals, and hence sulphides analysed during this study were only associated with olivine and pyroxene (herein referred to as 'carbonate-absent sulphides'). In contrast, sample E19 has abundant carbonate-filled (carbonatitic) vugs and pockets (± plagioclase, granular/skeletal chromite and apatite), and the sulphides analysed from this sample occurred within, or at the edge of, these carbonate pockets (Fig. 7a–b; herein referred to as 'carbonate-present sulphides'). Carbonate-absent sulphides (i.e., R2) have a higher chalcopyrite abundance than carbonate-present sulphides (i.e., E19; see Table 2, Supplementary Table D and Fig. 7). We can also make a clear distinction between carbonate-absent *vs.* carbonate-present sulphides using trace element composition (see Section 4.4). However, unlike the Loch Roag suite of xenoliths, we cannot distinguish between sulphide groups according to the internal textures of mixed base metal sulphides in each setting, as in all cases sulphides display complex intergrown textures between Cu- and Ni–Fe endmembers (although with varying chalcopyrite abundance; e.g., Fig. 7b–f).

In the Streap Com'laidh xenoliths there appears to be only a single group of sulphide minerals as we cannot differentiate between sulphides on textural evidence. All sulphide grains are 60–200 µm in diameter, interstitial to olivine, pyroxene and spinel, and have similar complex intergrowths of chalcopyrite, pentlandite and pyrrhotite to that seen in the Rinibar Suite (although carbonate pockets are absent here) — see Fig. 8a–d and Supplementary Table D. Small Ni–Fe sulphide droplets (<2 µm in diameter) can also be seen nucleating on the edges of clinopyroxene and spinel (hercynite) that have themselves been partially melted (Fig. 8e–f). This is particularly the case at the margin of Streap Com'laidh xenoliths. These micron-scale sulphide droplets were too small to analyse by LA-ICP-MS and were not considered further in this study.

4.3.2. South of the GGF

As described in Section 4.1, some altered lherzolite xenoliths from south of the Great Glen (Patna, Islay, and probably Colonsay) preserve traces of the original peridotite silicate mineral textures (often with minor relic clinopyroxene and spinel). Despite this alteration, base metal sulphides are still readily observed in these xenoliths and have varying textures (see Supplementary Table D): For example, xenoliths from Colonsay have mixed base metal sulphides, always interstitial to the (pseudomorphed) silicates (Fig. 9a–e) and with unusual 'feather-like' intergrowths of chalcopyrite and

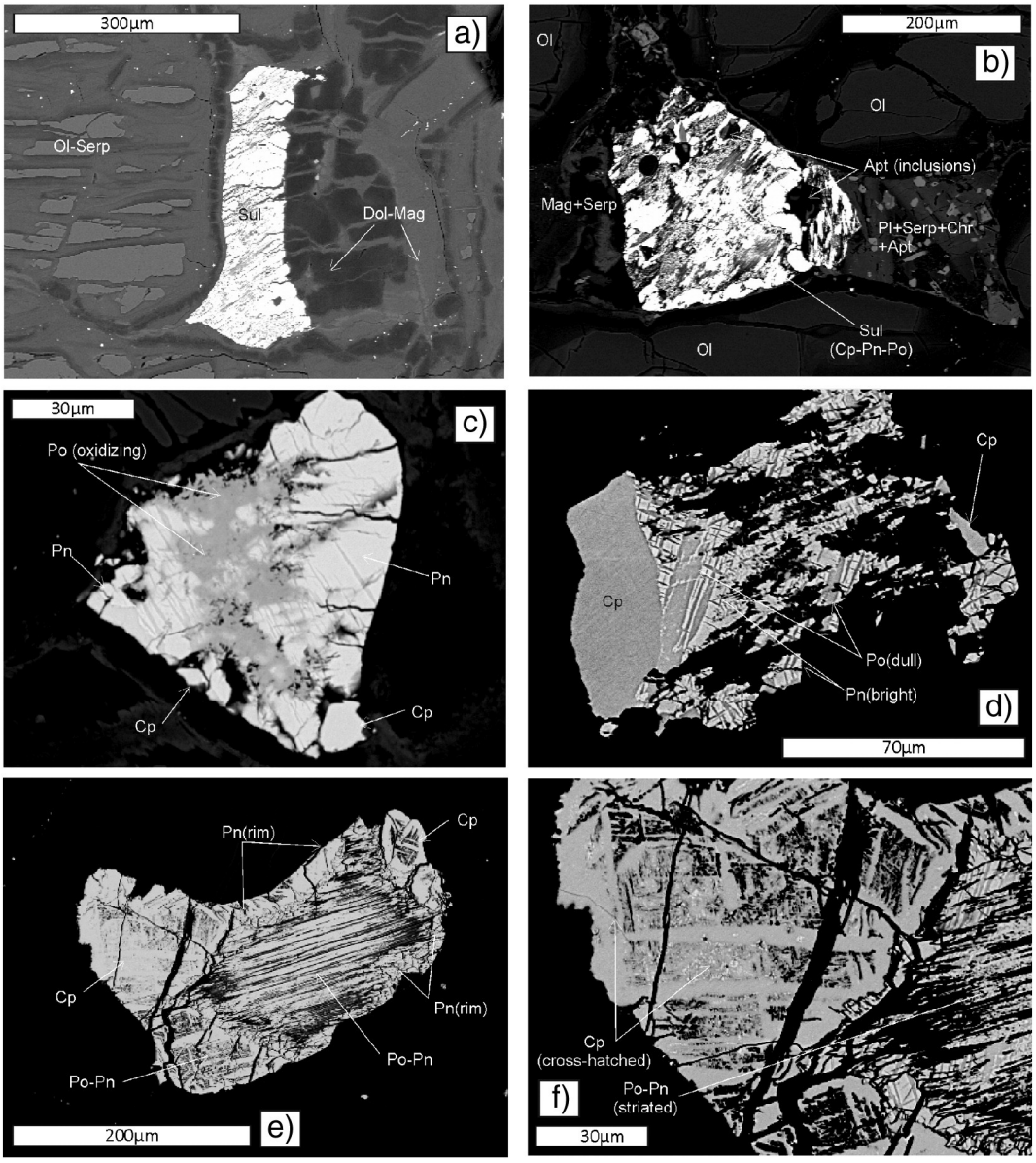

Fig. 7. Rinibar xenolith SEM backscatter electron images (BSE). (a) Elongate sulphide at the margin of a carbonate pocket and in contact with a serpentinised olivine crystal. Carbonates consist of intergrown dolomite and magnesite (sample E19). (b) Sulphide at the margin of a carbonate pocket (left hand side) and melt pocket (right hand side) inbetween granular serpentinised olivine crystals (sample E19). Carbonate pocket comprises magnesite, with minor serpentine probably entrained from the neighbouring olivines. The melt pocket consists of finely crystalline plagioclase, chromite and apatite, with accessory serpentine. Apatite inclusions occur within the sulphide globule. Sulphide minerals within the globule include chalcopyrite, pentlandite and pyrrhotite. (c) Sulphide at silicate triple junction (sample R2) — carbonate is absent. Contrast adjusted to show two outer edges of intergrown chalcopyrite and pentlandite with a central 'dappled' zone of pyrrhotite which is partially oxidising on the top left hand edge (sample R2). (d) Another example of a partially oxidising sulphide showing original chalcopyrite and cross-hatched intergrown pentlandite and pyrrhotite, which now has a dappled, skeletal and 'frayed' appearance as a result of partial melting (sample R2). (e) Mixed base metal sulphide (sample R2) showing multiple and complex textures within the grain. Carbonate is absent from this sample. (f) Close-up of left hand side of sulphides in (e) showing cross-hatched and granular appearance of chalcopyrite, next to striated pentlandite–pyrrhotite. Note the fine granular chalcopyrite and pentlandite crystals in the lower right hand corner of this image. This exemplifies the multiple generations of sulphide crystal growth associated with an 'aggregate' of sulphides. Mineral abbreviations are: olivine (Ol), serpentine (Serp), clinopyroxene (CPX), dolomite (Dol), magnesite (Mag), plagioclase (Pl), chromite (Chr), apatite (Ap), iron oxides (Fe-ox), orthoclase (Kfs), biotite (Bt), ilmenite (Ilm), pentlandite (Pn), chalcopyrite (Cp), pyrrhotite (Po).

pentlandite–pyrrhotite at the edge of Ca-carbonate and serpentine replacement zones (Fig. 9f–h). Millerite (NiS) is only observed as micron-scale, rounded, occasionally skeletal grains. Millerite is in all xenoliths which have pervasive replacement of silicates, particularly by quartz (e.g., Coire na Ba; Fig. 10a–b). Coire na Ba samples are generally sulphide-poor, but where present, sulphides consist of 2–5 µm diameter millerite grains although these were not large enough for LA-ICP-MS analyses.

Xenoliths from Islay typically contain simple monomineralic sulphides of rounded- to irregular-shape (up to 30 µm diameter). These are generally of Co-rich pentlandite and chalcopyrite, but pyrrhotite is often absent. Samples from Patna have Ni-Fe-Co-rich sulphides, <50 µm in diameter, which are rounded to irregular in shape. However less common 80–120 µm sized chalcopyrite grains (irregular shaped) are also observed in the Patna suite.

Sulphides are almost entirely absent from the Hillhouse xenoliths, despite the fresh mineralogy of this suite. In this respect, the Hillhouse spinel lherzolites are distinctive. However, rare droplets (<5 µm in diameter) of Ni-Fe sulphide occur around some margins of partially melted chromite, analogous to those of Streap Com'laidh.

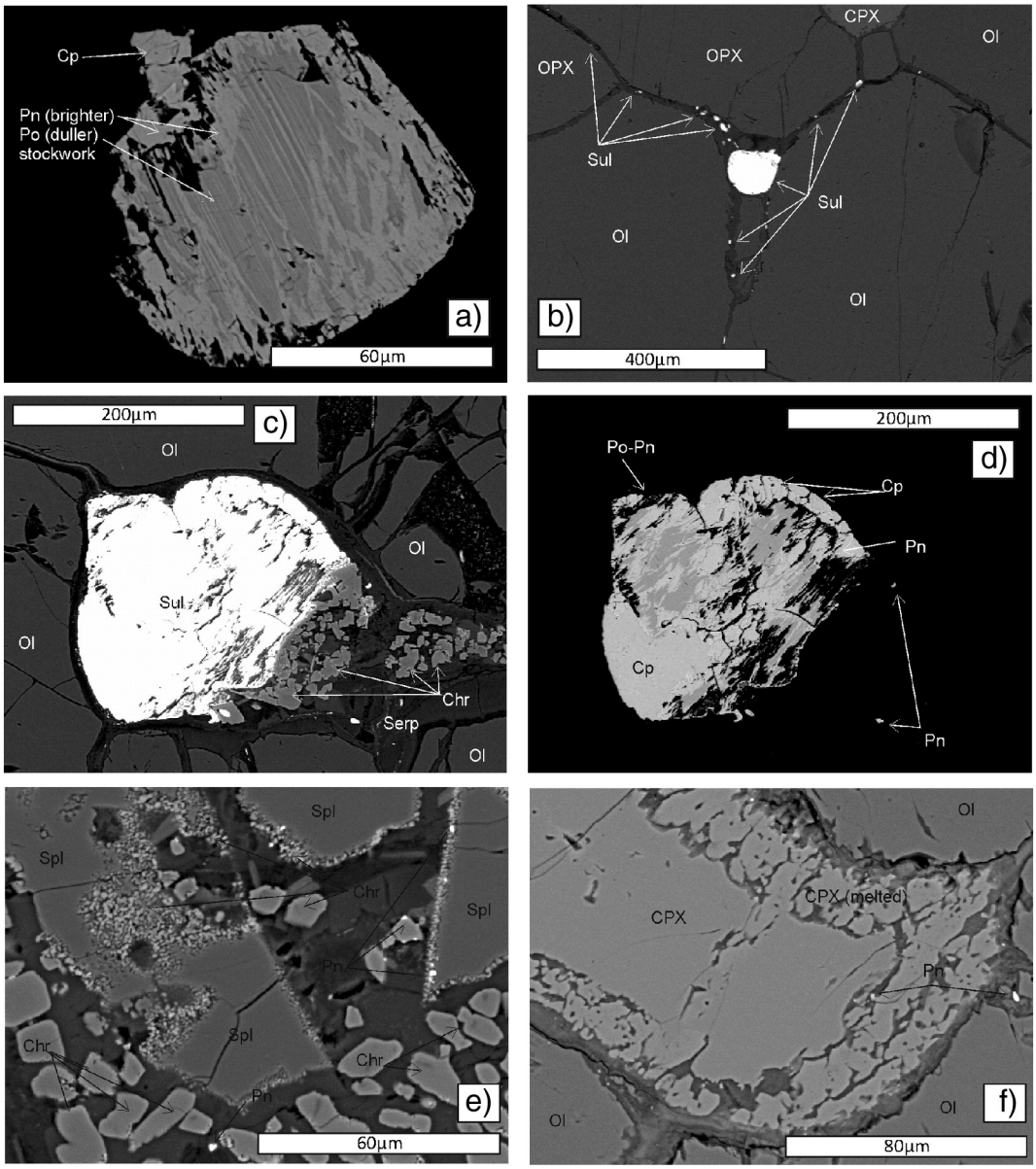

Fig. 8. Streap Com'laidh xenolith SEM BSE images. (a) Stockwork texture between pentlandite and pyrrhotite with minor chalcopyrite as distinct non-intergrown phases. Overall this is an example of a rounded sulphide globule. (b) Large rounded sulphide globule at olivine-orthopyroxene triple junction. Also note trail of µm-scale sulphides along silicate grain boundaries. (c) Sulphide at olivine grain boundaries (left) which is reacting on the right hand side to a more striated and irregular form. This reacting side is associated with fine-grained granular chromite within a pocket of serpentine. (d) The same sulphide as (c) with the contrast adjusted to display the sulphide internal texture and mineral phases. Note the rim of chalcopyrite *vs.* the central portion of intergrown pentlandite and pyrrhotite in a stockwork texture. (e) Al-Mg spinel melting at rim and forming granular chromite. Note the two crystal size populations of chromite: >5 µm granular, sub-euhedral chromite crystals *vs.* µm-scale rounded chromites. Both chromite populations are associated with µm-scale pentlandite globules at crystal margins. (f) Protogranular clinopyroxene and olivine. Clinopyroxene is melting to form finger-like crystals at its margins. This melt zone is again associated with µm-scale pentlandite globules. Note that (e) and (f) also appear in Hughes et al. (2015b). Mineral abbreviations are: clinopyroxene (CPX), orthopyroxene (OPX), olivine (Ol), spinel (Spl), chromite (Chr), serpentine (Serp), pentlandite (Pn), chalcopyrite (Cp), pyrrhotite (Po).

In summary, aside from the number of sulphide groups or populations observed in each xenolith suite, sulphide minerals occur in much greater abundance (and are generally coarser) north of the GGF compared with south of the GGF. We note that xenoliths from the Midland Valley (e.g., Patna and Hillhouse) have particularly low sulphide abundances.

4.4. Sulphide compositions

The trace element compositions of fifty-seven sulphide grains from spinel lherzolite xenoliths were analysed *in situ* by LA-ICP-MS (Supplementary Table E) and compared with seventy-seven sulphide grains analysed from Loch Roag (Hughes, 2015). In the geochemical plots of Figs. 11–14, data has been grouped according to xenolith terrane, except for the two Loch Roag sulphide 'populations' which are so distinct from one another (according to their texture *and* composition), that they span a greater range of compositions than all the other xenolith sulphides included in this study.

Due to variable grain size, mixed textures of base metal sulphides (BMS), and the nature of 'incision' by the laser, LA-ICP-MS analyses commonly incorporated multiple sulphide phases resulting in mixed spectra (i.e., pentlandite mixed with pyrrhotite and/or chalcopyrite, etc). To account for these mixed spectra, results in Supplementary Table E have been classed according to their major BMS end-member (pyrrhotite, Po; pentlandite, Pn; chalcopyrite, Cp) - see footnote to Fig. 11.

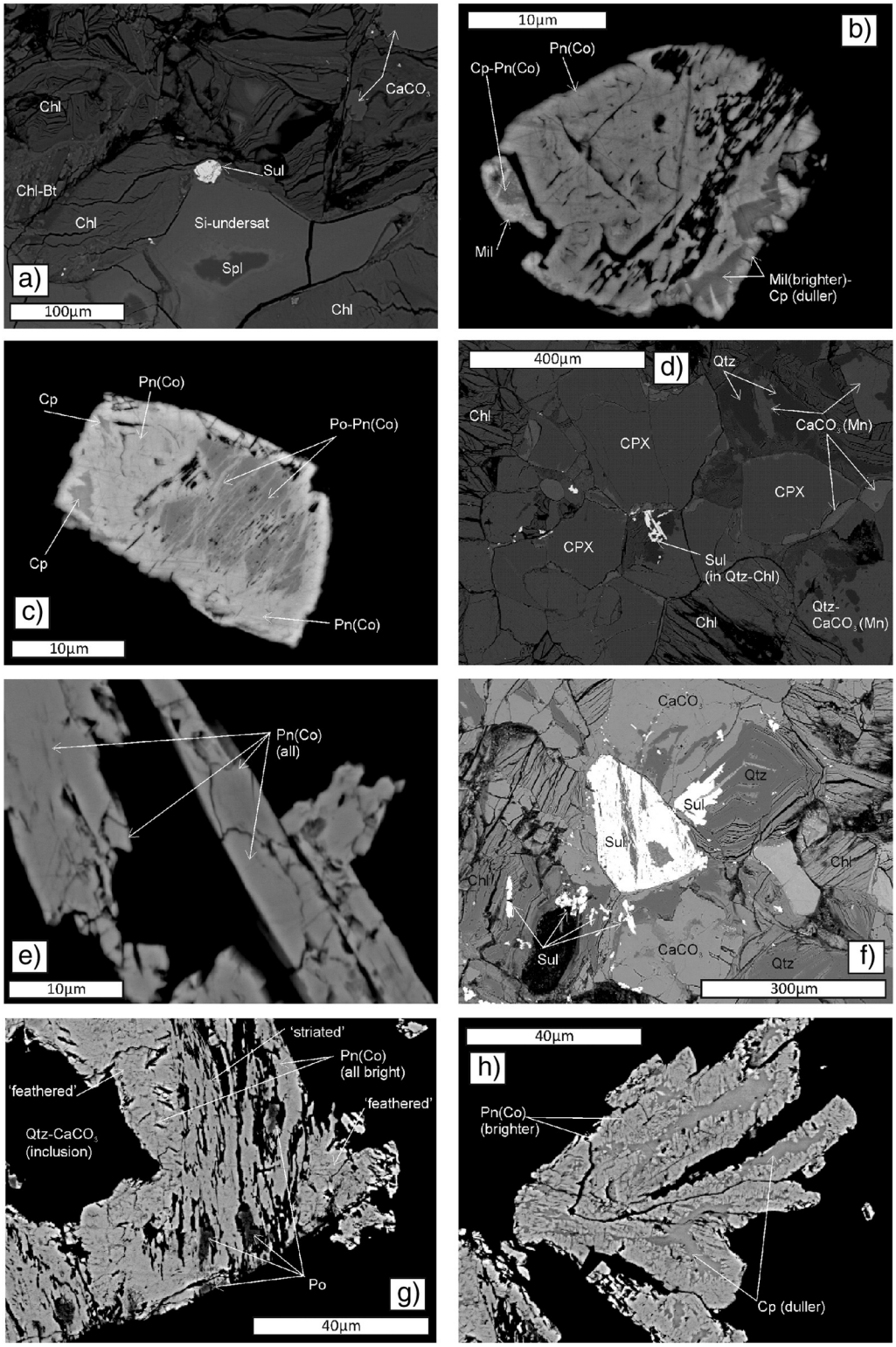

Fig. 9. Colonsay xenolith SEM BSE images. (a) Al-Mg spinel as relic cores surrounded by wide crystal margins or rims of an unidentified Si-bearing phase of similar Al, Mg, Cr, Fe content to the true spinel core. This has SiO_2 content up to only 13 wt.%, and is therefore not a spinel nor feldspathoid. Rounded sulphide is at Si-rich spinel margins (probably the original spinel margin) and surrounded by serpentine (partially replaced by chlorite) with minor biotite. Minor patches of Ca-carbonate also noted in chlorite. (b) Close-up image of sulphide in (a) showing complex sulphide textures. Co-bearing pentlandite (probably colbaltpentlandite) with millerite and chalcopyrite as intergrown phases in flame-like or stockwork texture. (c) Complex texture of blocky sulphide multi-phase crystal. Chalcopyrite and colbaltpentlandite as coarser phases around the edge of a fine stockwork of pyrrhotite and cobaltpentlandite. (d) Skeletal sulphide within a quartz-serpentine (chlorite) intergrowth and as an embayment within granular clinopyroxene. Clinopyroxene is surrounded by further serpentine and chlorite and quartz-Ca(Mn)-carbonate intergrowths. (e) Close-up of skeletal sulphide in (d) showing internal 'granular' texture of cobaltpentlandite. (f) Coarse irregular to skeletal shaped sulphide (multi-phase) in quartz-Ca-carbonate intergrowths (which have replaced original 'primary' silicates of the xenolith) and with serpentine/chlorite. (g) Close-up of lower right hand side of main sulphide in (f) showing 'feathered' and 'striated' textures in cobaltpentlandite, with minor elongate inclusions of pyrrhotite. Note quartz-Ca-carbonate inclusion on left hand side of image. (h) Close-up of branched sulphide on right hand side of (f) showing intergrown 'feathered' almost 'dendritic' texture between chalcopyrite (appears duller) and cobaltpentandite (appears brighter). Mineral abbreviations are: serpentine and/or chlorite (Chl), biotite (Bt), quartz (Qtz), Ca-carbonate or calcite ($CaCO_3$), Ca(Mn)-carbonate ($CaCO_3$(Mn)), clinopyroxene (CPX), cobaltpentlandite (Pn(Co)), chalcopyrite (Cp), pyrrhotite (Po), millerite (Mil).

Total PGE + Re + Au abundance does not appear to strictly correlate with any BMS 'class' (e.g., Po, Pn, Cp, etc; Fig. 11a–b). Overall the highest total PGE + Re + Au abundances are in sulphides from the Grampian Terrane, a sub-set from the Patna suite (Midland Valley Terrane), and Loch Roag 'droplet sulphides' (Hebridean Terrane). Sulphides from the Northern Highland Terrane have moderate total PGE + Re + Au contents, greater than Loch Roag 'complex sulphides'.

Colonsay sulphides appear to have a bimodal spread of data for Co, such that sulphides in a xenolith from one of the two xenolith-bearing monchiquite dykes on the island ('CRB' dyke; see Supplementary Table D) has low Co (<4500 ppm) whilst xenolith sulphides from the other xenolithic dyke ('COD' dyke) have extremely high abundances of Co (3 to 4.6 wt.%). This split in Colonsay data is irrespective of the proportion of Cu-, Fe- or Ni-rich end-member per analyses.

Extreme elevation in Co abundance in sulphides is ubiquitous in xenolith suites from south of the Great Glen Fault (GGF), although not always in millerite. In contrast sulphides from xenolith suites north of the GGF entirely lack this enrichment, and Co is only present in trace abundances (<6000 ppm; Fig.11c–d). For xenolith sulphides from north of the GGF, Co appears to gradually increase with increasing Ni and decreasing Cu content, although this is only ever at parts per million (ppm) levels. In contrast, for high-Co sulphides from south of the GGF, Co does not strictly correlate with Ni, although there is a broad positive correlation with Cu. There is no correlation between Co and Fe north of the GGF but there is to the south (Fig. 11e), where Fe-poor sulphides have the highest Co abundance.

In summary, Co concentration appears to be an important discrimination parameter for xenolith suites from either side of the GGF. There is no correlation between total PGE and Co abundances for any xenolith suites analysed during this study (cf. Fig. 11a and c) and the high-Co sulphides from xenoliths south of the GGF have a similar range of total PGE abundances to the Loch Roag 'droplet sulphides'.

4.4.1. Platinum-group element geochemistry

4.4.1.1. North of the GGF. As shown by Hughes (2015) and Section 4.3, two sulphide groups are identified on textural grounds in Loch Roag xenoliths ('complex sulphides' and 'droplet sulphides'). These have distinct PGE and Re compositions, such that 'complex sulphides' have the lowest PGE abundances and highest $(Re/Os)_N$ ratios (>1), whilst 'droplet sulphides' have the highest PGE concentrations and the lowest $(Re/Os)_N$ ratios (<1). Some 'droplet sulphides' have rounded carbonate inclusions within them but do not differ geochemically (trace element composition) from the rest of the 'droplet sulphides' where inclusions are absent. We compare the composition of sulphides from other Scottish xenolith suites to those established for the Loch Roag suite, by plotting the mean 'complex' and 'droplet' sulphide compositions on each chondrite-normalised (McDonough and Sun, 1995) diagram in Fig. 12.

Overall, sulphide compositions in xenoliths from the Northern Highland Terrane (Rinibar and Streap Com'laidh) have a similar PGE abundance to 'droplet sulphides' from Loch Roag, as IPGE are not depleted relative to PPGE (Fig. 12a–c), and $(Re/Os)_N$ ratios, although variable, range 0.3 to 7.4 (Supplementary Table E). Other sulphide groupings identified on the basis of textural features (i.e., presence or absence of carbonate in the Rinibar suite) show subtle variations in composition. Carbonate-present (E19) Rinibar sulphides are predominantly composed of pentlandite and pyrrhotite (with a minor chalcopyrite component), whilst carbonate-absent (R2) Rinibar sulphides have notably more chalcopyrite. Further, carbonate-absent (R2) Rinibar sulphides (Fig. 12a) have IPGE contents ranging ~10 to 50 × chondrite and $(Re/Os)_N$ ratios ~ 1 (Supplementary Table E). In contrast, carbonate-present (E19) Rinibar sulphides have much more variable IPGE abundances (~1–50 × chondrite) and generally higher $(Re/Os)_N$ ratios (>1) — see Fig. 12a and b, Supplementary Table E. Overall, carbonate-present (E19) sulphides have more variable *total* PGE abundances (approximately 1 × chondrite) than carbonate-absent (R2) sulphides, although there is significant overlap (10–89 ppm and 45–78 ppm respectively). Pt *vs.* Pd is variable in carbonate-present (E19) sulphides (Fig. 12b), with negative anomalies in Pt indicative of early formation of a Pt-bearing platinum-group mineral (PGM) that differentiated from the sulphide (cf. McDonald, 2008) and/or which was not analysed by the laser. Hence ^{195}Pt spikes in time resolution analyses (TRA in Supplementary Material, and also evident as positive Pt anomalies in Fig. 12b) from some LA-ICP-MS analyses of these samples indicate that Pt-bearing PGM (possibly cooperite; PtS) are strictly associated with carbonate-present (E19) sulphide grains in the Rinibar suite.

The trace element compositions of the Streap Com'laidh sulphides are most akin to carbonate-absent (R2) Rinibar sulphides, although Streap Com'laidh sulphides have a greater range of normalised-IPGE fractionation patterns (Fig. 12c). Pt and Pd anomalies are also quite variable in Streap Com'laidh sulphides (Fig. 12c) and could suggest that discrete Pt-bearing PGM may also be present in these xenoliths. However, we note that Streap Com'laidh sulphides have a higher pentlandite component, and this may be partly responsible for the negative Pt anomalies in Fig 12c.

4.4.1.2. South of the GGF. In the Grampian terrane, sulphides in Colonsay xenoliths (Fig. 12d) generally have PGE patterns similar to those of Streap Com'laidh and carbonate-absent (R2) Rinibar analyses, with approximately 1–100 × chondrite concentrations. Most Colonsay sulphide analyses also show negative Pt anomalies. Sulphides from Islay xenoliths (Fig. 12e) have the highest average PGE abundances, with 10–200 × chondrite (except for Pt). Apart from one analysis, most Islay sulphides display negative Pt anomalies. Au is less variable in the Grampian Terrane sulphides than those of the Northern Highland Terrane (which possess both strong positive and negative anomalies; cf. Fig. 12a–c *vs.* d–e).

Sulphides from Patna (Midland Valley Terrane) display the most variable PGE patterns analysed (Fig. 12f), although we note that many Patna sulphides were too small for LA-ICP-MS analysis (<30 μm). All Patna sulphides have a negative Pt anomaly, but otherwise their chondrite-normalised PGE patterns are highly variable and appear to define two groups; one with elevated PPGE and a strong negative Au anomaly *vs.* one with PPGE depletion and no Au anomaly (Fig. 12f). These groups do not correspond with any systematic difference in Ni-, Cu- or Fe-abundance or base metal mineral group dominance, and neither is there a systematic difference in Co enrichment.

4.4.1.3. Host dyke sulphides. Sulphides in the mafic host dykes are generally Ni-Fe sulphides or Fe-only sulphides, although some Cu–Fe sulphides have been noted in the basaltic clasts of the Patna breccia pipe. In all cases, the sulphides have very low abundances of PGE (typically below detection limit for LA-ICP-MS) and Co (<350 ppm).

4.4.2. Other trace elements in sulphides

A plot of Co *vs.* Zn shows that the content of Zn in sulphides from north of the GGF varies over five orders of magnitude (from 5 to 20,000 ppm) whilst Co remains low (<6000 ppm: Fig. 13a). Sulphides with >1000 ppm Zn have more variable Co abundances whereas most sulphides from south of the GGF, with very high Co contents, have <2000 ppm Zn.

As indicated in Section 4.4.1, $(Re/Os)_N$ can be used as a crucial discrimination factor for the Loch Roag sulphides ('complex' *vs.* 'droplet' in this study, and e.g., Hughes, 2015). In Fig. 13b, all xenoliths from the Northern Highland, Grampian and Midland Valley Terranes have $(Re/Os)_N$ values ranging 0.1 to 10 and are similar to 'Loch Roag droplet sulphides', although we note that the Northern Highland, Grampian and Midland Valley Terrane sulphides have slightly higher Os abundances.

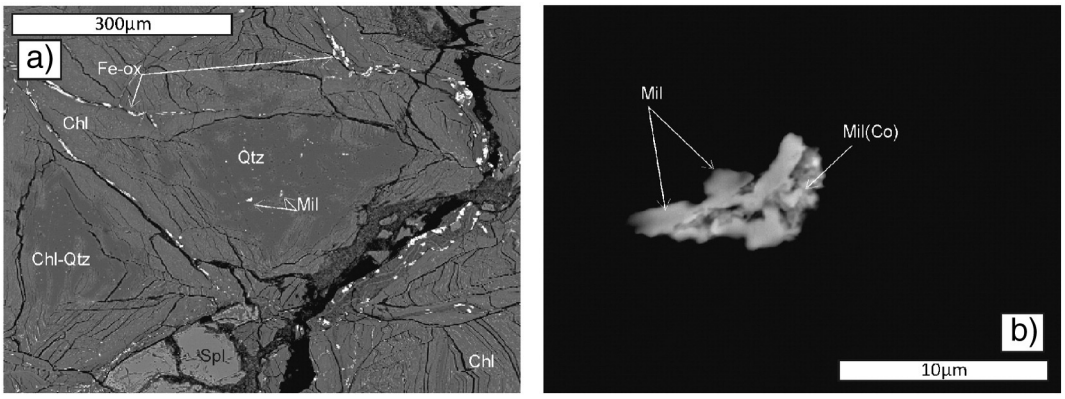

Fig. 10. Coire na Ba xenolith SEM BSE images. (a) Tiny millerite grains are inclusions in quartz. Quartz is intergrown with serpentine and chlorite (with accessory iron oxide). (b) Close-up image of a millerite grain, showing skeletal texture and areas of Co-bearing millerite (appearing brighter). Mineral abbreviations are: quartz (Qtz), serpentine and/or chlorite (Chl), iron oxide (Fe-ox), millerite (Mil), Co-bearing millerite (Mil(Co)).

5. Terrane-scale trends in sulphide petrography and precious metals

5.1. Sulphide mineral abundance and 'populations'

Multiple coexisting sulphide populations with different textures, PGM associations and trace element contents, together with the overall abundance of coarse grained (>50 µm) sulphide minerals (that are sometimes carbonate-associated) appear to be common characteristics of the xenoliths from north of the GGF. South of the GGF, sulphides are finer-grained, less complex texturally, and appear to lack discrete PGM. These features mirror the age of the lithosphere (Archaean *vs.* Proterozoic or younger) from which xenoliths were derived. Overall the terranes and their associated lithospheric mantle keels are thought to become younger (and less complex) from north to south in Scotland (Upton et al., 2011). Hence, the sulphide mineralogy and PGE geochemistry of the lithospheric mantle across the region may reflect the wider geodynamic regime in the same way as the chemistry of the SCLM (delineated by SCLM-derived lamprophyric magmas (cf. Canning et al., 1996, 1998).

Various studies of mantle lithologies have shown that the PGE budget is largely controlled by sulphides, due to PGE chalcophile behaviour: IPGE are thought to be mainly hosted by Fe-rich monosulphide solid solution and/or refractory metal alloys where there has been significant partial melting (Brenan and Andrews, 2001; Sattari et al., 2002; Bockrath et al., 2004; Luguet et al., 2007; Maier et al., 2012; Lorand et al., 2013 and references therein). PPGE are thought to be predominantly hosted by interstitial Cu-rich sulphides (Bockrath et al., 2004; Lorand et al., 2013; Sattari et al., 2002 and references therein). Accordingly, interstitial Cu-rich sulphides transfer into the silicate melt first during mantle partial melting and Pd and Pt are lost from the residual mantle, leaving a restite depleted in these elements (e.g., Maier et al., 2012 and references therein). The lower bulk rock Pt, Pd and Cu abundances in Greenlandic NAC xenoliths (Wittig et al., 2010) compared with Scottish NAC xenoliths (Figs. 2b and 4a) may reflect greater melt extraction from the Greenlandic NAC lithospheric mantle. Alternatively, and given the evidence of multiple 'populations' of sulphides in the Loch Roag suite (Fig. 6), this difference in bulk composition may instead represent significant refertilisation of the Scottish xenoliths. The latter come from the margin of the NAC (Fig. 1b) – this setting is most likely to have experienced Palaeoproterozoic refertilisation (possibly associated with the Nagssugtoqidian event in Greenland; e.g., Hughes et al., 2015a,b) – see further details in Section 5.2. Accordingly, whilst the widely accepted model for bulk PGE behaviour tracking that of sulphur may be valid for the asthenosphere, it may not strictly follow for the lithospheric mantle, where added complexities in the form of coexisting sulphide assemblages with different vulnerabilities to lithospheric melting may have significant bearing (e.g., Delpech et al., 2012; Guo et al., 1999; Hughes et al., 2015a; Lorand et al., 2004).

5.2. Metasomatism north of the GGF: Sulphide-carbonate-phosphate immiscibility and Pt-enrichment

'Droplet sulphides' from Loch Roag xenoliths have discrete micron-sized PtS grains (cooperite) within them (Fig. 6b). It is likely that this cooperite formed as a result of Pt-saturation in the sulphide droplets as they crystallised (Holwell and McDonald, 2010) — thus the sulphide liquid that formed these droplets was not only PGE-rich, but specifically Pt-rich. Some 'droplet sulphides' also preserve rounded inclusions of Ca-carbonate (Fig. 6c) and we suggest that this is a rare preserved example of sulphide-carbonate immiscibility, possibly associated with carbonatitic melts. Further, we document 'spongy' apatite crystals which have abundant inclusions of Ca-carbonate and micron-sized Ni-Fe-(Cu) sulphides (Fig. 6d), demonstrating sulphide-carbonate-phosphate immiscibility recorded in the Loag Roag suite.

In Rinibar xenoliths we find 'pockets' of carbonates and/or apatite with skeletal chromite grains associated with sulphides (Fig. 7a–b). Sulphides are sometimes seen with rounded apatite inclusions (e.g., Fig. 7b). These carbonate-present sulphides often have spikes in Pt content when analysed by LA-ICP-MS and we suggest that this is caused by discrete Pt-rich PGM present within the sulphide grain (similar to Loch Roag 'droplet sulphides'). Thus, the carbonate-phosphate association (either as inclusions *within* sulphides, or as carbonate-sulphide-apatite 'pockets') is evidence for widespread carbonatitic melts having passed through the SCLM north of the GGF. Given the association of this three-way immiscibility with sulphides carrying discrete Pt-bearing PGM, it appears likely that this carbonatitic metasomatism contributed to the Pt-enrichment of the SCLM north of the GGF.

In many instances, cratonic xenoliths are PPGE-depleted, but in some cases re-introduction of Pd by transient silicate melts and/or oxidising fluids linked to metasomatism has been invoked (e.g., Lorand et al., 2008 a,b; McInnes, 1999; Pearson et al., 2003). Based on 'primary' and 'metasomatic' clinopyroxene compositions identified in xenolith suites from north of the GGF (Hughes et al., 2015b) and time-integrated Sr- and Nd-isotopic studies for Loch Roag xenoliths (Long et al., 1991) we suggest that this metasomatism was pre-Permian in age, and probably occurred in the Precambrian. Further, this metasomatism was not restricted to mobilising only Pd, as exemplified by the discrete PtS observed in Loch Roag and Rinibar. We suggest that Pt-enrichment in the northern Scottish terranes thus represents a later (metasomatic) influx of sulphide liquid refertilising the shallow lithospheric mantle here.

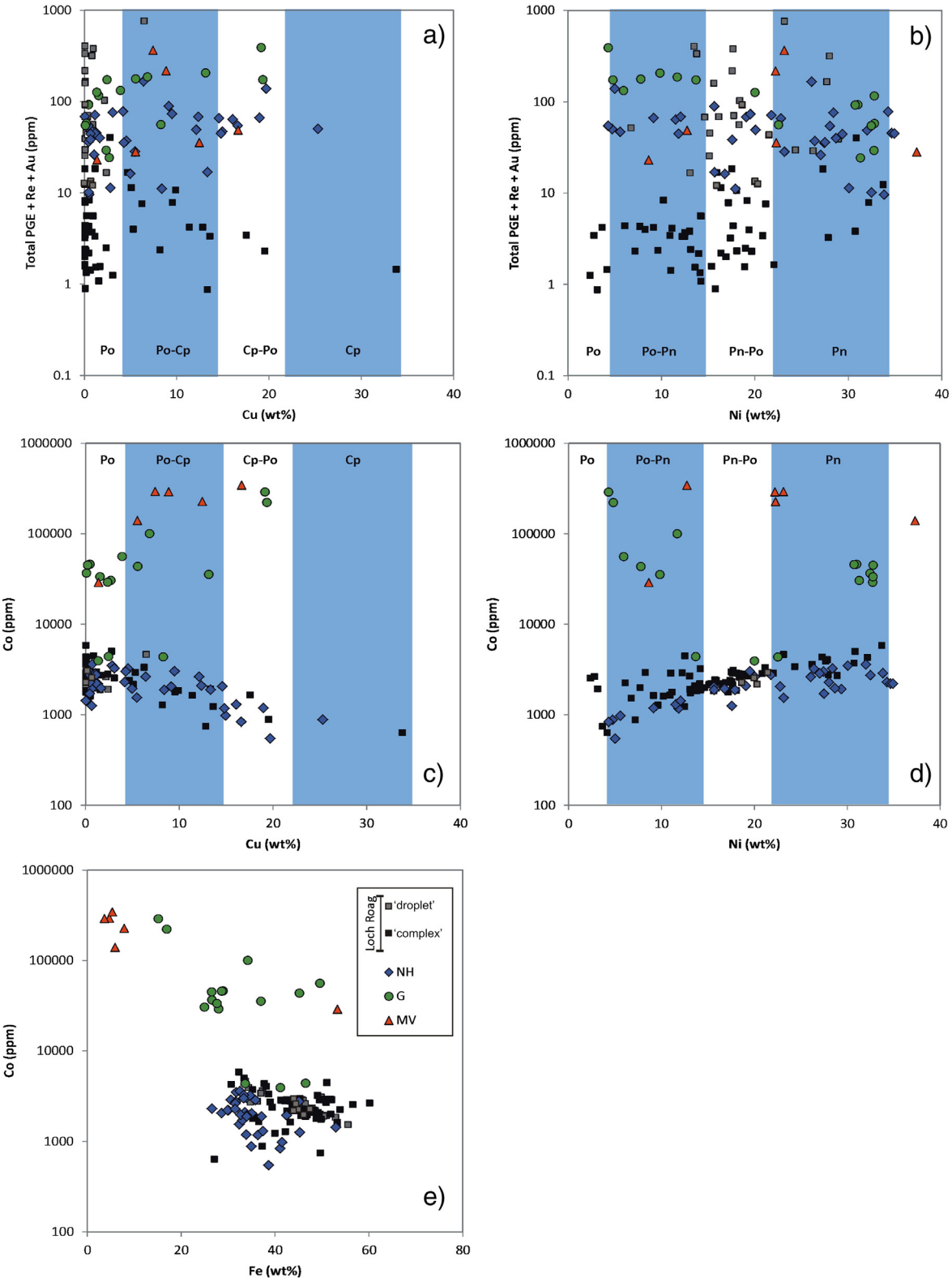

Fig. 11. Sulphide chalcophile element composition bivariant plots for total PGE + Re + Au *vs.* Cu (a) and Ni (b). Co *vs.* Cu (c) and Co *vs.* Ni (d). Also Co *vs.* Fe (e). Data is divided according to terrane (Northern Highland = NH, Grampian = G, Midland Valley = MV). For Loch Roag (Hebridean Terrane) data have been divided according to two sulphide populations (as described by Hughes, 2015); 'complex' *vs.* 'droplet' sulphides. LA-ICP-MS data. Analyses with < 5 wt.% Ni + Cu are classified as Po; 5–15 wt.% Ni or Cu are Po-Pn or Po-Cp respectively; 15–22 wt.% Ni or Cu are Pn-Po or Cp-Po respectively; and analyses with ≥ 22 wt.% Ni or Cu are classified as Pn or Cp. In results where both Ni and Cu abundances are > 5 wt.% each, analyses have been labelled Cp-Pn or Pn-Cp (depending on which metal is dominant). This classification scheme distinguishes details of trace element compositions of Cp, Pn and Po end members of each 'population' of sulphides and/or per xenolith suite.

Similar 'pockets' of sulphide-carbonate have been observed in Kerguelen mantle xenoliths (e.g., Delpeche et al., 2012; Lorand et al., 2004; Moine et al., 2004). Apatite-rich xenoliths are described by O'Reilly and Griffin (2000)) and apatite-rich layers (sometimes with carbonate 'aggregates') occur in Alpine ophiolitic peridotite (Morishita et al., 2008). In both of these cases, apatite

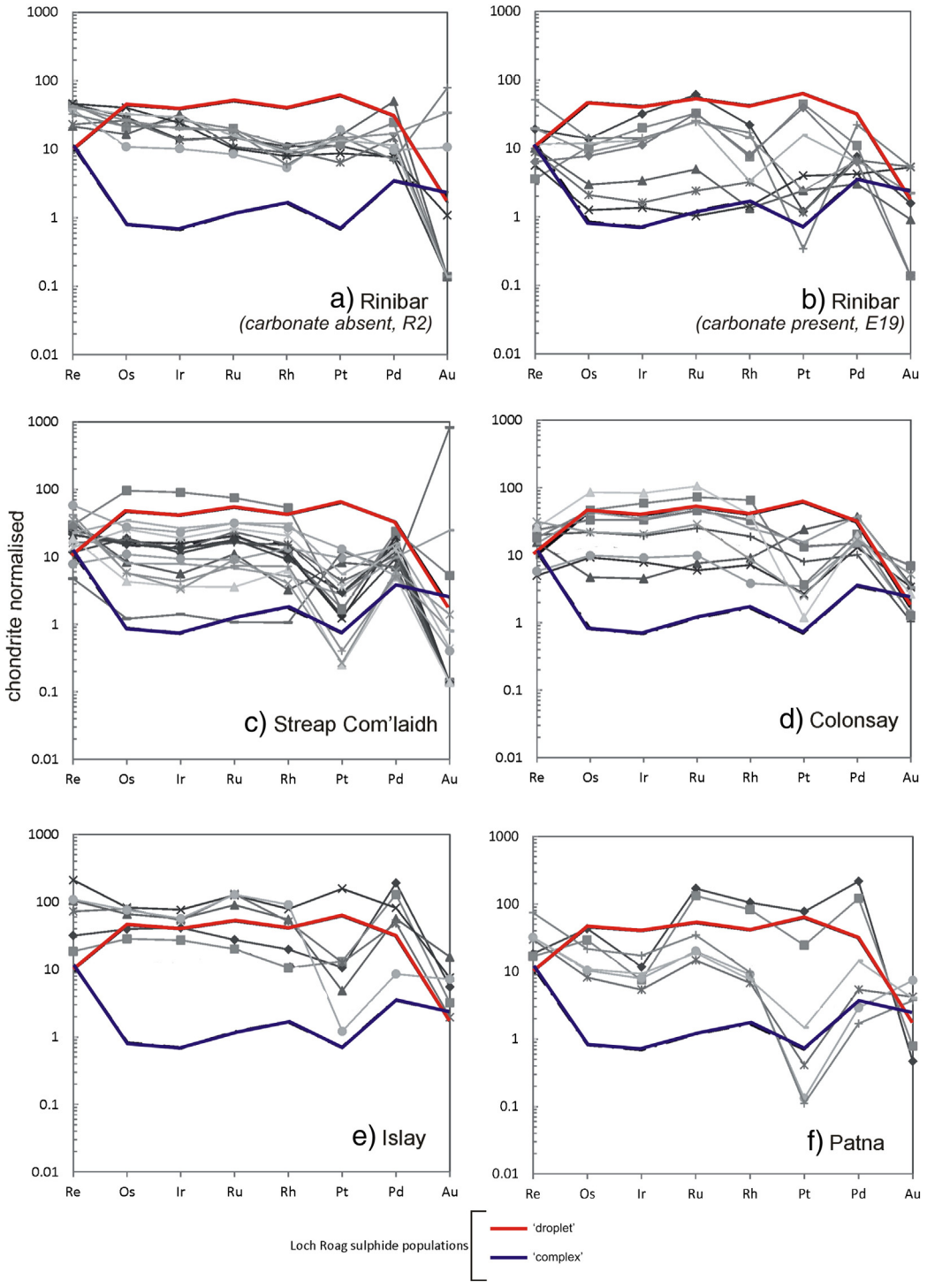

Fig. 12. Sulphide PGE multi-element diagrams per xenolith suite (chondrite normalised; McDonough and Sun, 1995); (a) Rinibar sulphides from carbonate-absent xenolith (sample R2), (b) Rinibar sulphides from carbonate-present xenolith (sample E19), (c) Streap Com'laidh, (d) Colonsay, (e) Islay and (f) Patna sulphides. All plots show mean sulphide compositions of 'complex' and 'droplet' sulphides from Loch Roag, for reference. LA-ICP-MS data.

(and carbonate) is thought to have resulted from metasomatism associated with major tectono-magmatic events. Morishita et al. (2008) suggest this was linked with a period of rifting, whereas the carbonate-sulphide associations of the Kerguelen xenoliths are thought to be related to mantle plume-derived carbonatites.

Only one carbonatite has been documented in the UK at Loch Urigill (Young et al., 1994), which may be related to the alkaline Loch Borralan intrusion (429.2 ± 0.5 Ma; Goodenough et al., 2011) and represent a small-scale partial melt from the lithospheric mantle. Carbonatite metasomatism has also been identified by Sr-, Nd-, and Hf-isotopic studies of Rinibar and Streap Com'laidh xenoliths (Bonadiman et al., 2008). Whether the carbonatitic magma was truly derived from the SCLM itself, or was transient through it, 'pockets' of carbonatitic affinity appear to have been preserved in xenoliths from the northern Scottish lithospheric mantle. We suggest that carbonatitic magmatism may therefore occur more widely in northern Scotland than current surface mapping might indicate. Crucially, the age and geodynamic environment associated with these Scottish carbonatitic melts have yet to be established.

Craton reconstructions in the North Atlantic show that the NAC was bordered to the north by the Nagssugtoqidian orogenic belt (1900–

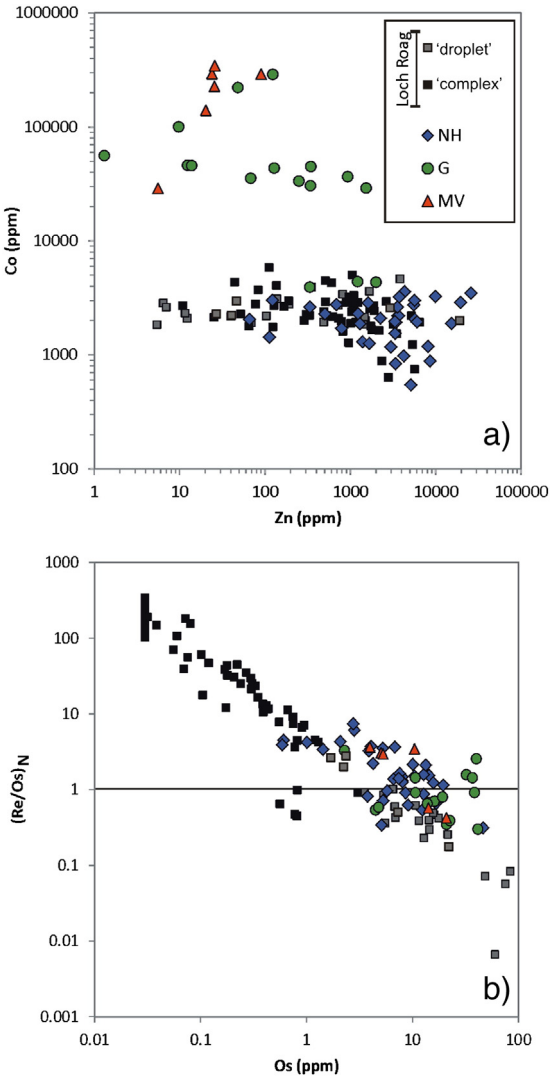

Fig. 13. Sulphide composition binary plots (LA-ICP-MS data); (a) Co *vs.* Zn and (b) $(Re/Os)_N$ *vs.* Os. Data is divided according to terrane (Northern Highland = NH, Grampian = G, Midland Valley = MV). For Loch Roag data (Hebridean Terrane), results have been divided according to sulphide population (as described by Hughes, 2015); 'complex' vs 'droplet' sulphides.

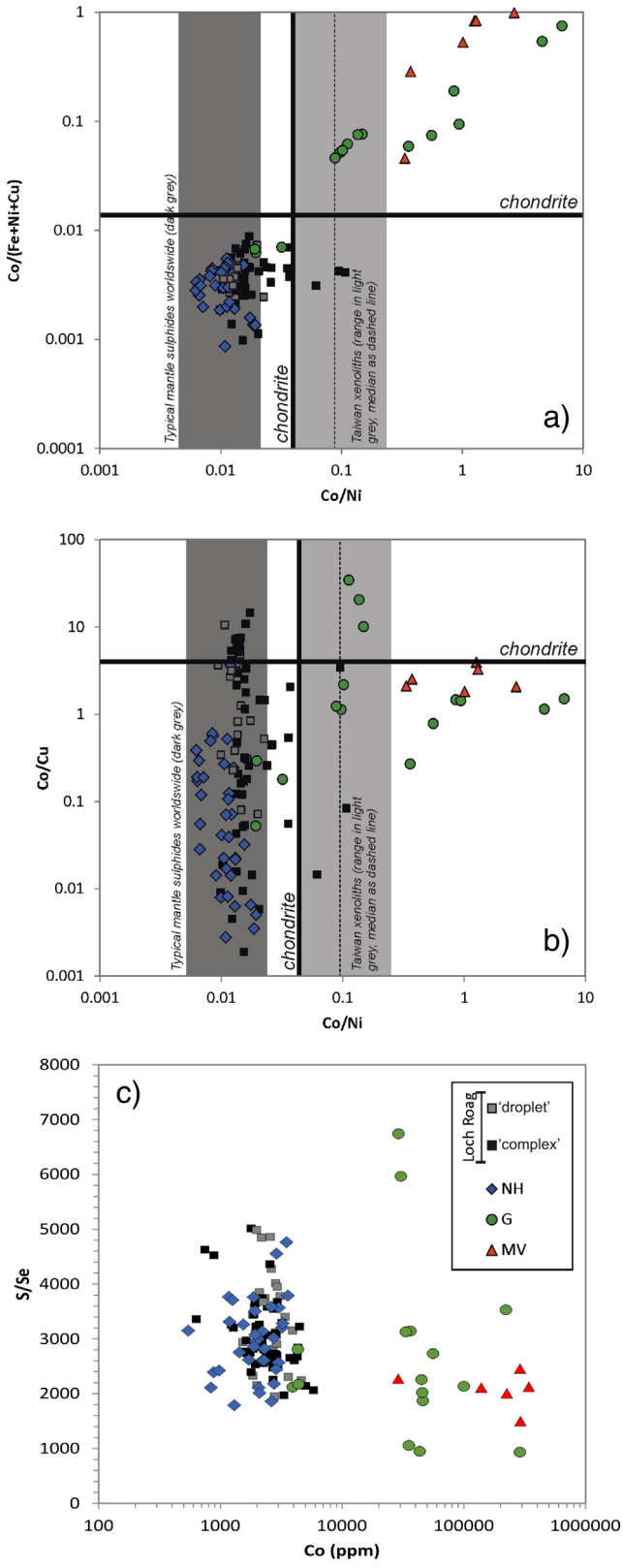

Fig. 14. Sulphide composition binary plots (LA-ICP-MS data) for Co; (a) Co/(Fe + Ni + Cu) ratio *vs.* Co/Ni ratio, (b) Co/Cu ratio *vs.* Co/Ni ratio; (c) S/Se ratio *vs.* Co. Chondritic ratios are labelled (from McDonough and Sun, 1995) as well as worldwide and Taiwanese sulphide Co/metal ratios (according to Wang et al., 2010).

1680 Ma; van Gool et al., 2002; Kolb, 2014) and that this Palaeoproterozoic mobile belt forms the southern border of the Rae Province. The Lewisian Gneiss Complex and its underlying SCLM occur on the very margin of the NAC and experienced Palaeoproterozoic orogenesis (e.g., accretion of Loch Maree arc terrane c. 1900 Ma; Park, 2002). SCLM Pt-enrichment appears to be restricted to lithospheric mantle lineaments such as cratonic block boundaries and their bordering (or overprinting) Palaeoproterozoic orogenic belts (cf. Hughes et al., 2015a). Thus Pt-enrichment may not be inherited from the bulk of the depleted keel, but is instead a feature restricted to shallow and re-fertilised cratonic margins. We highlight that whole-rock PGE data alone may mask details pertaining to subtleties in sulphide population(s). Whilst the whole-rock Pt/Pd ratio of cratonic xenoliths may be broadly chondritic (Fig. 4a) we can demonstrate that specific sulphides within these xenoliths (namely those associated with carbonate-phosphate-sulphide immiscibility and situated within cross-cutting spinel-feldspar symplectites) are Pt-rich.

Overall, sulphides in xenoliths from north of the GGF have some of the highest Pt/Pd ratios recorded across Scotland frequently with Pt/Pd > chondrite (Supplementary Table E). In contrast, sulphides with some of the highest total PGE abundances exist in xenoliths from south of the GGF, but crucially these also have a sub-chondritic Pt/Pd ratio. This could reflect a sampling bias relating to the relative number

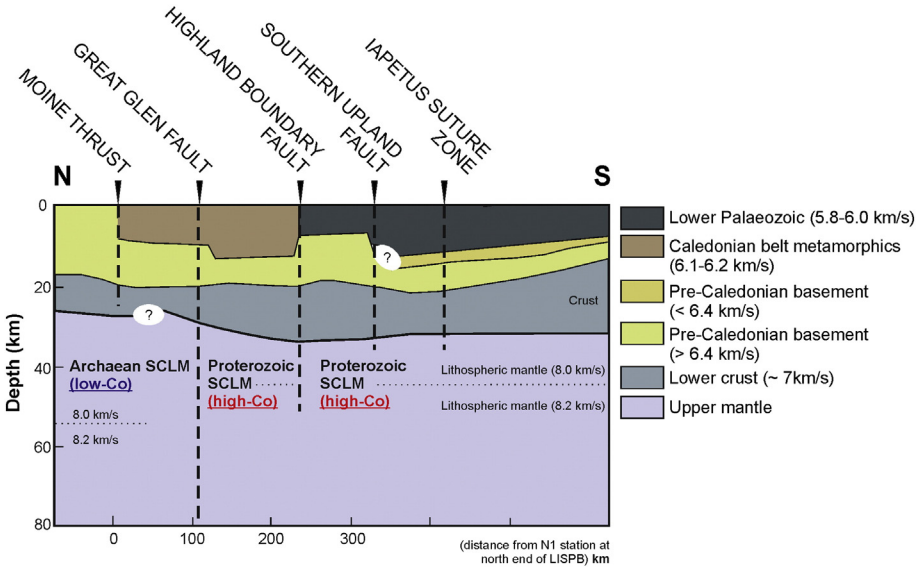

Fig. 15. Schematic model showing lithospheric mantle below Scotland and the distribution of Archaean (cratonic) SCLM with low-Co sulphides (north of the GGF) *vs.* Proterozoic (or younger) SCLM with high-Co sulphides (south of the GGF). Seismic velocities and north-south section adapted from Bamford et al. (1978).

of Cu- *vs*. Ni-rich sulphides analysed, as Cu-sulphides are typically depleted in Pd relative to Ni-sulphides (see Holwell and McDonald, 2010). However, we find no correlation between Pt/Pd ratios and Cu content for sulphides across the xenoliths suites. Nonetheless, if Pt-enrichment is specific to the ancient carbonatite-metasomatised SCLM of the craton margins, the *lack* of Pt-enrichment (and therefore relative Pd-enrichment) of the southern Scottish xenoliths upholds the inference that they represent lithospheric mantle formed in an entirely different (non-cratonic) setting.

The abundances of precious metals and chalcophile elements at the margin of the NAC in northern Scotland (as recorded in Loch Roag and Rinibar xenoliths) were unaffected by Phanerozoic overprinting, either in the Permo-Carboniferous or Palaeogene tectono-magmatic event (Hughes et al., 2015b). But in the Palaeogene, the process of lithospheric mantle delamination (e.g., Kerr, 1994; Saunders et al., 1997) may have led to the assimilation and incorporation of Loch Roag-type sulphides (Pt-rich sulphide populations) — as demonstrated by the changing Pt/Pd ratio of North Atlantic Igneous Province lavas from continental to oceanic rifting (Hughes et al., 2015a).

6. Cobalt and the Great Glen Fault — a major lithospheric lineament distinction

A clear division can be seen between Co concentrations in sulphides in xenoliths from north and south of the GGF. Xenoliths from the north have only trace levels of Co in all their base metal sulphides whilst those from the south are significantly Co-enriched (typically several weight percent). North of the GGF most xenolith sulphides have sub-chondritic Co/chalcophile element ratios (i.e., Co/Ni and Co/(Fe + Ni + Cu)) that contrast with super-chondritic Co/chalcophile element ratios in those from the south (Fig. 14a). The chondritic Co/Cu ratio is 4.2 (McDonough and Sun, 1995) and we see no spatial correlation for Co/Cu ratios of sulphides on either side of the GGF (Fig.14b). This suggests that Co preferably follows Ni and Fe and is not coupled with Cu nor affected by sulphide liquid fractionation during cooling.

Two Permo-Carboniferous dykes host the spinel lherzolites on Colonsay, but no previous work has been published on the xenolith suites they contain. However, based on the abundance of Co in sulphides in xenoliths from each dyke, coupled with Colonsay's position straddling the GGF, we tentatively suggest that xenoliths from these two dykes may represent different but neighbouring terranes — the Northern Highland (north) and Grampian (south) Terranes.

Co-rich sulphides analysed in this study occur along grain boundaries and the majority of southern xenolith silicate minerals are variably altered or replaced (e.g., peridotite silicate textures have been preserved by pervasive replacement of carbonates and quartz). This raises the question of whether alteration has also affected the sulphide minerals and produced the Co-enrichment, especially given the petrographic setting of the sulphides. There is no petrographic evidence for oxidation or break-down of sulphide minerals in the southern xenoliths. Sulphide oxidation would lead to sulphur loss that should be identifiable from the S/Se ratio (e.g., Lorand et al., 2003). Whereas S/Se ratios of the high-Co sulphides may in some cases be nominally lower (minimum 930) than most other Scottish xenolith sulphides (1700 to 5000) Co enrichment is not correlated with S/Se ratio (Fig.14c).

We observed micron-scale millerite grains in quartz pseudomorphs (e.g., Coire na Ba xenoliths; Fig. 10) but these low-temperature (hydrothermal?) sulphides are only rarely Co-rich (Fig. 10b). Hydrothermal sulphides would also be expected to have high S/Se ratios (as little Se would be available in this low-temperature system). Only two sulphide analyses (from the Grampian Terrane) have S/Se ratios substantially elevated above 5000, and these have approximately 2 wt.% Co (Fig. 14c). Whilst it is possible that the breakdown of Co-bearing silicates, such as olivine, may release Co which is subsequently taken up by sulphides, Co enrichment is not strictly tallied with the degree of xenolith alteration. Crucially, the style of alteration among the southern xenolith suites is highly variable (Table 1) and Co-rich sulphides occur in all the southern suites, regardless of the alteration style. Further, in many cases olivine has been preserved despite alteration in other portions of a xenolith (e.g., clinopyroxene).

We also discount the possibility of such alteration resulting from pervasive replacement of silicates by fluids derived from host dykes because the sulphides in the host dykes have extremely low Co (<350 ppm; Supplementary Table E). The abundance of sulphide minerals is also unlikely to explain their Co content — whilst we observe that sulphides are generally smaller and are in lower abundances in western Scottish xenoliths from south of the GGF (in comparison to those from the north) we cannot identify a trend between sulphide grain size and Co concentration in the high-Co sulphides. Hence we suggest that the Co-rich sulphides are a primary feature of the lithospheric mantle, and not an artefact of alteration. This Co-enrichment of sulphides may not be identified in bulk geochemistry if sulphide

abundances are low, as the whole-rock Co budget may be dominated by silicates (olivine). Nonetheless, we tentatively highlight an elevated whole-rock Co/Ni ratio in Patna xenoliths (Table 2).

To our knowledge only three examples of Co-rich sulphides in mantle xenoliths and xenocrysts are available in the published literature: these are a) peridotitic sulphide inclusions in micro-diamonds (Lac de Gras, Slave Craton; Davies et al., 2004), b) sulphide grains in xenocrystic olivine and pyroxenes (Lac de Gras, Slave Craton; Aulbach et al., 2004) and c) serpentinised and carbonatised peridotite xenoliths from Taiwan (Wang et al., 2010). For the micro-diamond inclusions, sulphides were recorded with up to 14.7 wt.% Co, whilst Lac de Gras xenolith sulphides have up to 13.1 wt.% Co. Sulphides from the Taiwan xenoliths (pervasively altered and pseudomorphed spinel lherzolites) have up to 11.5 wt.% Co. Hence sulphides in xenoliths south of the GGF have the highest recorded Co compositions reported globally thus far (up to 34.3 wt.% Co). Due to the association of sulphides with micro-diamonds and xenolith assemblages from kimberlites, the elevation in Co in the Lac de Gras sulphides could indicate a fundamental control by mantle plume magmatism (e.g., Aulbach et al., 2004 and Davies et al., 2004). The Taiwanese xenolith sulphides have similarly been suggested to be derived from deep mantle plume magmatism based primarily on the high $^{3}He/^{4}He$ composition of the xenoliths (Wang et al., 2010). However, two neighbouring suites of xenoliths were studied by Wang et al. (2010) and only one of these contained sulphides with elevated Co. Therefore we question the likelihood of a deep plume signature only being recorded in one of these suites, both of which were entrained and erupted in lavas at similar times (16–8 Ma and 13–10 Ma; see Wang et al., 2010 and references therein). Given the lack of comparable data, we are cautious in our interpretation of the implications for such Co-rich sulphides — perhaps these are generally underreported due to the similar lack of sulphide-specific studies of mantle xenoliths, as well as being specific to a certain tectonic or geodynamic environment. The relationship of Co-enrichment strictly to a mantle plume setting remains ambiguous, and in the case of the Scottish xenoliths, there is no evidence of a Permo-Carboniferous mantle plume (Kirstein et al., 2004).

Cobalt may be associated with various mineralisation settings and is normally mined as a by-product with other sulphide-hosted metals. Of particular relevance to this work are massive and disseminated sulphides in serpentinised (and often carbonated) ultramafic bodies in Morocco (Bou Azzer; e.g., Leblanc and Fischer, 1990; Ahmed et al., 2009), Finland (Outokumpu; e.g., Peltonen et al., 2008), and the Urals (Ivanovka and Ishkinino; see Peltonen et al., 2008 and references therein). As yet there is no well-defined deposit model to categorise this style of mineralisation and modern analogues for these deposits have not been clearly identified. However, we note that high Co concentrations are also associated with Mn-nodules and chemical sediments on the seafloor and oceanic crust (e.g., Burns, 1976; Calvert and Price, 1970; Glasby, 2006). Coupled with Co-rich sulphides in hydrothermal Cu–Zn–Co–Au–(Ni) peridotite-floored deposits of slow-spreading ridges (e.g., the Logatchev and Rainbow fields, Mid-Atlantic Ridge; Bogdanov et al., 1997, Murphy and Meyer, 1998 and Douville et al., 2002) this provides intriguing information about the geodynamic environment associated with such Co mineralisation — namely oceanic lithosphere (e.g., Ahmed et al., 2009).

In Scotland, Co mineralisation is documented in a number of settings (see Hannis and Bide, 2009). The oldest known Co-bearing mineralisation is associated with Fe and Ni–Cu–As sulphides in Late Caledonian (Silurian) appinite- and diorite-bearing intrusions, such as Talnotry (Southern Uplands; Power et al., 2004) and Sron Garbh (Tyndrum, Grampian Terrane; Graham et al., 2013) where PGM have also been reported. Late Carboniferous polymetallic veins, sometimes cross-cutting strata-bound Zn-Pb deposits in the Midland Valley and Grampian Terranes, can also be associated with Co mineralisation (at Silver Glen near Alva, Hilderston, Coille-bhraghad and Tyndrum — e.g., Coats et al., 1982; Hall et al., 1982; Stephenson et al., 1983; Pattrick, 1985). In these cases there is often an association of Co with As, Ag and sometimes Au. Indeed we see a similar association of Co-enrichment with elevated As and Ag in sulphides from xenoliths (see Supplementary Material).

In all of these Scottish mineralised settings, metals such as Ni, Cu and Co are thought to be mantle-derived and appinites (e.g., Sron Garbh) are the direct products of lithospheric mantle melting (e.g., Platten, 1999 and references therein). Crucially, all of these documented occurrences of Co mineralisation occur south of the GGF. This is particularly pertinent because there are analogous Late Caledonian appinitic intrusions bearing Co-poor sulphides and PGM on the northern side of the GGF (e.g., Loch Borralan Complex; Styles et al., 2004). Hence it appears that the Co-rich nature of the Scottish mantle xenoliths from southern terranes is complimented by Co-bearing mineralisation south of the GGF. The question arises: what controls this terrane-scale Co-enrichment?

The global association between ophiolite fragments, serpentinised/carbonated ultramafic pod-like bodies (e.g., Outokumpu, Finland) and Co-enrichment may be inherent to a fluid-rich oceanic rifting environment or seafloor sedimentary setting. If the Co-rich mantle beneath southern Scotland is the subducted relic of formerly rifted (Iapetus) oceanic lithosphere, then given the Permo-Carboniferous ages of xenolith entrainment and the oldest Co-bearing mineralisation associated with Silurian appinites, the rifting must have pre-dated the Caledonian orogeny. Iapetus oceanic crust formation was associated with the opening of the Iapetus Ocean and rifting of Rodinia c. 600 Ma in Scotland (see Trewin, 2002 and references therein). Serpentinised and PGM-bearing ophiolitic material (south of the GGF) is documented near the Southern Upland Fault at Ballantrae and along the Highland Boundary Fault (e.g., at Corrycharmaig; Power and Pirrie, 2000, 2004). It is currently not clear as to whether sulphides in these ophiolitic bodies are also enriched in Co (or at least if chemical sediments of the ophiolitic packages are Co-enriched) but the model outlined above predicts that they should be.

Overall, given the significant lateral movement along the GGF (estimated to be 1200 km during Caledonian orogenesis between Laurentia and Baltica; Dewey and Strachan, 2003) prior to Permo-Carboniferous entrainment of xenolith suites, and the cratonic lithospheric keel beneath northern Scotland; we find that sulphide compositions, petrography and textures can distinguish between lithospheric mantle regions (Fig.15). These regions directly correspond with crustal terranes that formed in various geodynamic settings. Although the age of sulphide minerals underlying the terranes of Scotland have yet to be quantitatively determined, we tentatively suggest that sulphide compositions may provide a thus far unexplored opportunity for metallogenic 'mapping' of the lithospheric mantle. Accordingly, we may make regional predictions regarding the 'prospectivity' of terranes for precious and critical metal mineralisation. In the case of Scotland (and thus potentially also Ireland) we predict that Co-rich mineralisation may be restricted to areas south of the GGF with mantle-derived magmatism also being relatively Pd-rich. In contrast, mantle-derived magmatism to the north of the GGF will be Co-poor and more Pt-enriched.

7. Conclusions

1. Sulphide mineral petrography and composition may be used to identify 'populations' of sulphide minerals from xenolith suites across a region, terrane or even co-existing within a single xenolith (e.g., Loch Roag). This is particularly the case of Archaean-Palaeoproterozoic lithospheric mantle, where numerous (transient) tectono-magmatic and/or metasomatic events may be recorded (e.g., Loch Roag and Rinibar, north of the GGF).
2. We find clear mineralogical evidence for carbonate-sulphide-phosphate immiscibility, and that this is associated with Pt-enrichment of sulphides (and occurrence of discrete Pt-bearing platinum-group minerals) in mantle xenoliths from Archaean-Palaeoproterozoic

terranes north of the GGF (e.g., Loch Roag and Rinibar). These highlight a significant PGE-rich sulphide-bearing carbonatitic event(s) in the lithospheric mantle underlying northern Scotland.
3. Terranes from south of the GGF record different sulphide compositions and textural characteristics. Pt/Pd ratios in xenolith sulphides south of the GGF are <chondrite and these have an extreme elevation in Co concentration (ranging 2.9 to 34.3 wt.%).
4. Cobalt concentration in the mantle (bulk and/or sulphide geochemistry) is generally under-reported. We suggest that Co-rich sulphides in the southern Scottish lithospheric mantle are recording a different geodynamic environment, intrinsic to Palaeozoic terranes south of the GGF, and contrasting with Archaean-Palaeoproterozoic terranes north of the fault. We tentatively propose that this Co enrichment is related to oceanic lithospheric mantle processes (cf., present day Mn-nodules and chemical sedimentary crusts) and that the younger lithospheric mantle below southern Scotland reflects this oceanic affinity.
5. A combined approach of sulphide morphology, composition (e.g., Co and PGE), radioisotopic geochronology, general sulphide petrographic setting (i.e., 'fusibility'; Hughes et al., 2015a), and mineralogical associations (e.g., carbonate and phosphate) provides a future opportunity for the metallogenic 'mapping' of the lithospheric mantle.

Supplementary data to this article can be found online at http://dx.doi.org/10.1016/j.lithos.2015.11.007.

Acknowledgements

Much of the material (xenolith and dyke) used throughout this study is from B.G.J. Upton's personal collection, now held at the British Geological Survey (BGS), Murchison House, Edinburgh. The BGS, particularly Michael Togher, is thanked for the curation, access and use of these samples. New samples from Streap Com'laidh were collected by J.W. Faithfull, and are henceforth curated at the Hunterian Museum, University of Glasgow. Anthony Oldroyd is thanked for his preparation of polished thin sections, and Peter Fisher and Duncan Muir for their assistance and guidance at Cardiff University's SEM facility. This manuscript greatly benefitted from discussions with Judith Coggon and Ambre Luguet. Kathryn Goodenough is particularly thanked for her patient and inspiring discussions, and detailed comments on an earlier manuscript and Katie Dobbie also provided valuable feedback. Two anonymous reviewers are thanked for their helpful and thorough reviews of the manuscript, and Nelson Eby is thanked for his editorial management. H.S.R. Hughes was funded by the Natural Environment Research Council (NERC) studentship NE/J50029X. NERC are thanked for funding open access publication of this paper.

References

Ahmed, A.H., Arai, S., Ikenne, M., 2009. Mineralogy and paragenesis of the Co–Ni arsenide ores of Bou Azzer, Anti-Atlas, Morocco. Economic Geology 104, 249–266.
Arndt, N.T., 2013. The lithospheric mantle plays no active role in the formation of orthomagmatic ore deposits. Economic Geology 108, 1953–1970.
Aulbach, S., Griffin, W.L., Pearson, N.J., O'Reilly, S.Y., Kivi, K., Doyle, B.J., 2004. Mantle formation and evolution, Slave Craton: constraints from HSE abundances and Re–Os isotope systematics of sulfide inclusions in mantle xenocrysts. Chemical Geology 208, 61–88.
Ballhaus, C., Tredoux, M., Spath, A., 2001. Phase relations in the Fe–Ni–Cu–PGE–S system at magmatic temperature and application to massive sulphide ores of the Sudbury Igneous Complex. Journal of Petrology 42, 1911–1926.
Bamford, D., Nunn, K., Prodehl, C., Jacob, B., 1978. LISPB—IV. Crustal structure of northern Britain. Geophysical Journal International 54 (1), 43–60.
Baxter, A.N., Mitchell, J.G., 1984. Camptonite-monchiquite dyke swarms of northern Scotland; age relationships and their implications. Scottish Journal of Geology 20, 297–308.
Bockrath, C., Ballhaus, C., Holzheid, A., 2004. Fractionation of the platinum-group elements during mantle melting. Science 305, 1951–1953.
Bogdanov, K., Tsonev, D., Kuzmanov, K., 1997. Mineralogy of gold in the Elshitsa massive sulphide deposit, Sredna Gora zone, Bulgaria. Mineralium Deposita 32, 219–229.
Bonadiman, C., Coltorti, M., Duggen, S., Paludetti, L., Siena, F., Thirlwall, M.F., Upton, B.G.J., 2008. Palaeozoic subduction-related and kimberlite or carbonatite metasomatism in the Scottish lithospheric mantle. In: Coltorti, M., Gregoire, M. (Eds.), Metasomatism in Oceanic and Continental Lithospheric Mantle. The Geological Society, London.
Brenan, J.M., Andrews, D., 2001. High-temperature stability of laurite and Ru–Os–Ir alloy and their role in PGE fractionation in mafic magmas. The Canadian Mineralogist 39, 341–360.
Brown, P.E., Dempster, T.J., Hutton, D.H.W., Becker, S.M., 2003. Extensional tectonics and mafic plutons in the Ketilidian rapakivi granite suite of South Greenland. Lithos 67, 1–13.
Burns, R.G., 1976. The uptake of cobalt into ferromanganese nodules, soils, and synthetic manganese (IV) oxides. Geochimica et Cosmochimica Acta 40, 95–102.
Calvert, S.E., Price, N.B., 1970. Geochemical variation in ferromanganese nodules and associated sediments from the Pacific Ocean. Marine Chemistry 5, 43–74.
Canning, J.C., Henney, P.J., Morrison, M.A., Gaskarth, J.W., 1996. Geochemistry of late Caledonian minettes from Northern Britain: implications for the Caledonian subcontinental lithospheric mantle. Mineralogical Magazine 60, 221–236.
Canning, J.C., Henney, P.J., Morrison, M.A., Van Calsteren, P.W.C., Gaskarth, J.W., Swarbrick, A., 1998. The Great Glen Fault: a major vertical lithospheric boundary. Journal of the Geological Society 155, 425–428.
Coats, J.S., Tandy, B.C., Michie, U.M., 1982. Geochemical drainage survey of central Argyll, Scotland. Mineral Reconnaissance Programme Report No. 50. Natural Environment Research Council.
Craig, J.R., Vaughan, D.J., 1994. Applications of ore microscopy in mineral technology. Ore Microscopy And Ore Petrology, 2 ed.
Crowley, Q.G., Key, R.M., Noble, S.R., 2015. High-precision U–Pb dating of complex zircon from the Lewisian Gneiss Complex of Scotland using an incremental CA-ID-TIMS approach. Gondwana Research 27 (4), 1381–1391.
Daly, J.S., Muir, R.J., Cliff, R.A., 1991. A precise U–Pb zircon age for the Inishtrahull syenitic gneiss, County Donegal, Ireland. Journal of the Geological Society 148, 639–642.
Davies, J.H.F.L., Heaman, L.M., 2014. New U–Pb baddeleyite and zircon ages for the Scourie dyke swarm: a long-lived large igneous province with implications for the Paleoproterozoic evolution of NW Scotland. Precambrian Research 249, 180–198.
Davies, R.M., Griffin, W.L., O'Reilly, S.Y., Doyle, B.J., 2004. Mineral inclusions and geochemical characteristics of microdiamonds from the DO27, A154, A21, A418, DO18, DD17 and Ranch Lake kimberlites at Lac de Gras, Slave Craton, Canada. Lithos 77, 39–55.
De Hoog, J.C.M., Gall, L., Cornell, D.H., 2010. Trace-element geochemistry of mantle olivine and application to mantle petrogenesis and geothermobarometry. Chemical Geology 270, 196–215.
Delpech, G., Lorand, J.-P., Gregoire, M., Cottin, J.-Y., O'Reilly, S.Y., 2012. In-situ geochemistry of sulfides in highly metasomatized mantle xenoliths from Kerguelen, southern Indian Ocean. Lithos 154, 296–314.
Dewey, J.F., Strachan, R.A., 2003. Changing Silurian–Devonian relative plate motion in the Caledonides: sinistral transpression to sinistral trantension. Journal of the Geological Society, London 160, 219–229.
Douville, E., Charlou, J.L., Oelkers, E.H., Bienvenu, P., Jove Colon, C.F., Donval, J.P., Fouquet, Y., Prieur, D., Approu, P., 2002. The rainbow vent fluids (36°14′N, MAR): the influence of ultramafic rocks and phase separation on trace metal content in Mid-Atlantic Ridge hydrothermal fluids. Chemical Geology 184, 37–48.
Faithfull, J.W., Timmerman, M.J., Upton, B.G.J., Rumsey, M.S., 2012. Mid-Eocene renewal of magmatism in NW Scotland: the Loch Roag Dyke, Outer Hebrides. Journal of the Geological Society 169, 115–118.
Friend, C.R.L., Strachan, R.A., Kinny, P.D., 2008. U–Pb zircon dating of basement inliers within the Moine Supergroup, Scottish Caledonides: implications of Archaean protolith ages. Journal of the Geological Society 165, 807–815.
Gillespie, M., Styles, M., 1999. BGS rock classification scheme. Classification Of Igneous Rocks. 1.
Glasby, G.P., 2006. Manganese: predominant role of nodules and crusts. In: Schulz, H.D., Zabel, M. (Eds.), Marine Geochemistry. Springer, Berlin Heidelberg.
Goodenough, K.M., Millar, I., Strachan, R.A., Krabbendam, M., Evans, J.A., 2011. Timing of regional deformation and development of the Moine Thrust Zone in the Scottish Caledonides: constraints from the U–Pb geochronology of alkaline intrusions. Journal of the Geological Society, London 168, 99–114.
Goodenough, K.M., Crowley, Q.G., Krabbendam, M., Parry, S.F., 2013. New U–Pb age constraints for the Laxford Shear Zone, NW Scotland: evidence for tectono-magmatic processes associated with the formation of a Paleoproterozoic supercontinent. Precambrian Research 233, 1–19.
Graham, S.D., Holwell, D.A., McDonald, I., Sangster, C., 2013. Pt contained within secondary pyrite – an example from Sron Garbh, an unconventional magmatic Cu-Ni-platinum group element prospect, Stirlingshire, Scotland. Applied Earth Science (Trans. Inst. Min. Metall. B) 122 (3), 149.
Groves, D.I., Bierlein, F.P., 2007. Geodynamic settings of mineral deposit systems. Journal of the Geological Society, London 164, 19–30.
Groves, D.I., Ho, S.E., Rock, N.M.S., Barley, M.E., Muggeridge, M.T., 1987. Archean cratons, diamond and platinum: evidence for coupled long-lived crust-mantle systems. Geology 15, 801–805.
Gunn, A.G., 2014. Critical Metals Handbook. John Wiley, Sons.
Guo, J., Griffin, W.L., O'Reilly, S.Y., 1999. Geochemistry and origin of sulphide minerals in mantle xenoliths: Qilin, Southeastern China. Journal of Petrology 40, 1125–1149.
Hall, I.H.S., Gallagher, M.J., Skilton, B.R.H., Johnson, C.E., 1982. Investigation of polymetallic mineralisation in Lower Devonian volcanics near Alva, central Scotland. Mineral Reconnaissance Programme Report No. 53. Natural Environment Research Council.
Hannis, S., Bide, T., 2009. Cobalt. Commodity Profile. British Geological Survey.
Hastie, A.R., Kerr, A.C., Pearce, J.A., Mitchell, S.F., 2007. Classification of altered volcanic island arc rocks using immobile trace elements: development of the Th Co discrimination diagram. Journal of Petrology 48, 2341–2357.

Hastie, A.R., Kerr, A.C., Mitchell, S.F., Millar, I.L., 2008. Geochemistry and petrogenesis of Cretaceous oceanic plateau lavas in eastern Jamaica. Lithos 101, 323–343.
Holwell, D.A., McDonald, I., 2010. A review of the behaviour of Platinum Group Elements within natural magmatic sulfide ore systems. Platinum Metals Review 54, 26–36.
Huber, H., Koeber, C., McDonald, I., Reimold, W.U., 2001. Geochemistry and petrology of Witwatersrand and Dwyka diamictites from South Africa: search for an extraterrestrial component. Geochimica et Cosmochimica Acta 65, 2007–2016.
Hughes, H.S.R., 2015. Temporal, Lithospheric And Magmatic Process Controls On Ni, Cu And Platinum-Group Element (PGE) Mineralisation: A Case Study From Scotland PhD thesis Cardiff University.
Hughes, H.S.R., McDonald, I., Goodenough, K.M., Ciborowski, T.J., Kerr, A.C., Davies, J.H.F.L., Selby, D., 2014. Enriched lithospheric mantle keel below the Scottish margin of the North Atlantic Craton: evidence from the Palaeoproterozoic Scourie Dyke Swarm and mantle xenoliths. Precambrian Research 250, 97–126.
Hughes, H.S.R., McDonald, I., Faithfull, J.W., Upton, B.G.J., Downes, H., 2015a. Trace element abundances in the shallow lithospheric mantle of the North Atlantic Craton margin: implications for melting and metasomatism beneath Northern Scotland. Mineralogical Magazine 79 (4), 875–906.
Hughes, H.S.R., McDonald, I., Kerr, A.C., 2015b. Platinum group element signatures in the North Atlantic Igneous Province: implications for mantle controls on metal budgets during continental breakup. Lithos 233, 89–110.
Ionov, D.A., Doucet, L.S., Carlson, R.W., Golovin, A.V., Korsakov, A.V., 2015. Post-Archean formation of the lithospheric mantle in the central Siberian craton: Re–Os and PGE study of peridotite xenoliths from the Udachnaya kimberlite. Geochimica et Cosmochimica Acta 165, 466–483.
Kerr, A.C., 1994. Lithospheric thinning during the evolution of continental large igneous provinces: a case study from the North Atlantic Tertiary province. Geology 22, 1027–1030.
Kinny, P.D., Friend, C.R.L., Love, G.J., 2005. Proposal for a terrane-based nomenclature for the Lewisian Complex of NW Scotland. Journal of the Geological Society, London 162, 175–186.
Kirstein, L.A., Dunai, T.J., Davies, G.R., Upton, B.G.J., Nikogosian, I.K., 2004. Helium isotope signature of lithospheric mantle xenoliths from the Permo-Carboniferous magmatic province in Scotland — no evidence for a lower-mantle plume. Geological Society, London, Special Publications 223, 243–258.
Kolb, J., 2014. Structure of the Palaeoproterozoic Nagssugtoqidian Orogen, South-East Greenland: model for the tectonic evolution. Precambrian Research 255, 809–822.
Leblanc, M., Fischer, W., 1990. Gold and platinum group elements in cobalt-arsenide ores: hydrothermal concentration from a serpentinite source-rock (Bou Azzer, Morocco). Mineralogy and Petrology 42.
Leggett, J.K., McKerrow, W.S., Eales, M.H., 1979. The southern uplands of Scotland: a Lower Palaeozoic accretionary prism. Journal of the Geological Society 136, 755–770.
Li, J., Agee, C.B., 1996. Geochemistry of mantle–core differentiation at high pressure. Nature 381, 686–689.
Li, C., Barnes, S.-J., Makovicky, E., Rose-Hansen, J., Makovicky, M., 1996. Partitioning of nickel, copper, iridium, rhenium, platinum, and palladium between monosulfide solid solution and sulfide liquid: Effects of composition and temperature. Geochimica et Cosmochimica Acta 60, 1231–1238.
Li, C., Ripley, E.M., 2009. Sulphur contents at sulfide-liquid or anhydrite saturation in silicate melts: empirical equations and example applications. Economic Geology 104, 405–412.
Long, A.M., Menzies, M.A., Thirlwall, M.F., Upton, B.G.J., Apsen, P., 1991. Carbonatite–mantle interaction: a possible origin for megacryst/xenolith suites in Scotland. In: Meyer, H.O.A., Leonardos, O.H. (Eds.), Fifth International Kimberlite Conference. Brazil.
Lorand, J.P., Alard, O., Luguet, A., Keays, R.R., 2003. Sulfur and selenium systematics of the subcontinental lithospheric mantle: inferences from the Massif Central xenolith suite (France). Geochimica et Cosmochimica Acta 67, 4137–4151.
Lorand, J.-P., Delpech, G., Gregoire, M., Moine, B., O'Reilly, S.Y., Cottin, J.-Y., 2004. Platinum-group elements and the multistage metasomatic history of Kerguelen lithospheric mantle (South Indian Ocean). Chemical Geology 208, 195–215.
Lorand, J.P., Luguet, A., Alard, O., 2008a. Platinum-group elements: a new set of key tracers for the Earth's interior. Elements 4, 247–252.
Lorand, J.-P., Luguet, A., Alard, O., Bezos, A., Meisel, T., 2008b. Abundance and distribution of platinum-group elements in orogenic lherzolites; a case study in a Fontete Rouge lherzolite (French Pyrénées). Chemical Geology 248, 174–194.
Lorand, J.-P., Luguet, A., Alard, O., 2013. Platinum-group element systematics and petrogenetic processing of the continental upper mantle: a review. Lithos 164–167, 2–21.
Love, G.J., Friend, C.R.L., Kinny, P.D., 2010. Palaeoproterozoic terrane assembly in the Lewisian Gneiss Complex on the Scottish mainland, south of Gruinard Bay: SHRIMP U–Pb zircon evidence. Precambrian Research 183, 89–111.
Luguet, A., Shirey, S.B., Lorand, J.-P., Horan, M.F., Carlson, R.W., 2007. Residual platinum-group minerals from highly depleted harzburgites of the Lherz massif (France) and their role in HSE fractionation of the mantle. Geochimica et Cosmochimica Acta 71, 3082–3097.
Maier, W.D., Peltonen, P., McDonald, I., Barnes, S.J., Barnes, S.J., Hatton, C., Viljoen, F., 2012. The concentration of platinum-group elements and gold in southern African and Karelian kimberlite-hosted mantle xenoliths: implications for the noble metal content of the Earth's mantle. Chemical Geology 302–303, 119–135.
McAteer, C.A., Stephen Daly, J., Flowerdew, M.J., Connelly, J.N., Housh, T.B., Whitehouse, M.J., 2010. Detrital zircon, detrital titanite and igneous clast U–Pb geochronology and basement–cover relationships of the Colonsay Group, SW Scotland: Laurentian provenance and correlation with the Neoproterozoic Dalradian Supergroup. Precambrian Research 181, 21–42.
McDonald, I., 2008. Platinum-group element and sulphide mineralogy from ultramafic complexes at Andriamena, Madagascar. Applied Earth Science, Transactions of the Institution of Mineralogy and Metallurgy, B 117, 1–10.
McDonald, I., Viljoen, K.S., 2006. Platinum-group element geochemistry of mantle eclogites: a reconnaissance study of xenoliths from the Orapa kimberlite, Botswana. Applied Earth Science 115, 81–93.
McDonough, W.F., Sun, S., 1995. The composition of the earth. Chemical Geology 120, 223–253.
McInnes, B.I., 1999. Osmium isotope constraints on ore metal recycling in subduction zones. Science 286, 512–516.
Menzies, M.A., Halliday, A.N., Hunter, R.N., MacIntyre, R.M., Upton, B.G.J., 1989. The age, composition and significance of a xenolith-bearing monchiquite dyke, Lewis, Scotland. In: O'Reilly, S.Y. (Ed.), Kimberlites and Related Rocks: their Mantle/Crust Setting, Diamonds and Diamond Exploration. Special Publication, Geological Society of Australia.
Moine, B., Gregoire, M., O'Reilly, S.Y., Delpech, G., Sheppard, S.M.F., Lorand, J.-P., Renac, C., Giret, A., Cottin, J.-Y., 2004. Carbonatite melt in oceanic upper mantle beneath the Kerguelen Archipelago. Lithos 75, 239–252.
Moorhouse, S.J., Moorhouse, V.E., 1977. A Lewisian basement sheet within the Moine at Ribigill, north Sutherland. Scottish Journal of Geology 13, 289–300.
Morishita, T., Hattori, K.H., Terada, K., Matsumoto, T., Yamamoto, K., Takebe, M., Ishida, Y., Tamura, A., Arai, S., 2008. Geochemistry of apatite-rich layers in the Finero phlogopite–peridotite massif (Italian Western Alps) and ion microprobe dating of apatite. Chemical Geology 251, 99–111.
Murphy, P.J., Meyer, G., 1998. A gold-copper association in ultramafic-hosted hydrothermal sulfides from the Mid-Atlantic Ridge. Economic Geology 93, 1076–1083.
Naldrett, A.J., 2011. Fundamentals of Magmatic Sulfide Deposits. In: Li, C., Ripley, E.M. (Eds.), Magmatic Ni-Cu and PGE Deposits: Geology, Geochemistry, and Genesis. Society of Economic Geologists, Reviews in Economic Geology. 17, pp. 1–51.
Ohtani, E., Yurimoto, H., Seto, S., 1997. Element partitioning between metallic liquid, silicate liquid, and lower-mantle minerals: implications for core formation of the Earth. Physics of the Earth and Planetary Interiors 100, 97–114.
Oliver, G.J.H., Wilde, S.A., Wan, Y., 2008. Geochronology and geodynamics of Scottish granitoids from the Neoproterozoic break-up of Rodinia to Palaeozoic collision. Journal of the Geological Society 165, 661–674.
O'Reilly, S.Y., Griffin, W.L., 2000. Apatite in the mantle: implications for metasomatic processes and high heat production in Phanerozoic mantle. Lithos 53, 217–232.
Palme, H., O'neill, H.S.C., 2004. Cosmochemical estimates of mantle composition. Treatise on Geochemistry 2, 1–38.
Park, R.G., 2002. The Lewisian Geology of Gairloch. NW Scotland, Geological Society, London.
Park, R.G., 2005. The Lewisian terraine model: a review. Scottish Journal of Geology 41, 105–118.
Pattrick, R.A.D., 1985. Pb–Zn and minor U mineralization at Tyndrum, Scotland. Mineralogical Magazine 49, 671–681.
Pearson, D.G., 2005. Mantle Samples Included in Volcanic Rocks: Xenoliths and Diamonds. In: Carlson, R.W. (Ed.), The Mantle And Core. Treatise On Geochemistry.
Pearson, D.G., Canil, D., Shirey, S.B., 2003. Mantle samples included in volcanic rocks: xenoliths and diamonds. Treatise on Geochemistry 2, 171–275.
Peltonen, P., Kontinen, A., Huhma, H., Kuronen, U., 2008. Outokumpu revisited: new mineral deposit model for the mantle peridotite-associated Cu–Co–Zn–Ni–Ag–Au sulphide deposits. Ore Geology Reviews 33, 559–617.
Pidgeon, R.T., Aftalion, M., 1978. Cogenetic And Inherited Zircon U–Pb Systems In Granites: Palaeozoic Granites Of Scotland And England. Scottish Academic Press Glasgow, Crustal evolution in northwestern Britain and adjacent regions.
Platten, I.M., 1999. Ardsheal hill and peninsula. In: Stephenson, D., Bevins, R.E., Millward, D., Highton, A.J., et al. (Eds.), Caledonian Igneous Rocks of Great Britain. JNCC.
Power, M.R., Pirrie, D., 2000. Platinum-group element mineralization within ultramafic rocks at Corrycharmaig, perthshire: implications for the origin of the complex. Scottish Journal of Geology 36, 143–150.
Power, M.R., Pirrie, D., 2004. Platinum-group minerals within the Ballantrae Complex, SW Scotland. Scottish Journal of Geology 40, 1–5.
Power, M.R., Pirrie, D., Jedwab, J., Stanley, J., 2004. Platinum-group element mineralization in an As-rich magmatic sulphide system, Talnotry, southwest Scotland. Mineralogical Magazine 68, 395–411.
Prichard, H.M., Knight, R.D., Fisher, P.C., McDonald, I., Zhou, M.-F., Wang, C.Y., 2013. Distribution of platinum-group elements in magmatic and altered ores in the Jinchuan intrusion, China: an example of selenium remobilization by postmagmatic fluids. Mineralium Deposita 48, 767–786.
Rehkamper, M., Halliday, A.N., Fitton, J.G., Lee, D.-C., Wieneke, M., Arndt, N.T., 1999. Ir, Ru, Pt and Pd in basalts and komatiites: new constraints for the geochemical behavior of the platinum-group elements in the mantle. Geochimica et Cosmochimica Acta 63, 3915–3934.
Rock, N.M.S., Groves, D.I., 1988. Can lamprophyres resolve the genetic controversy over mesothermal gold deposits? Geology 16 (6), 538–541.
Sattari, P., Brenan, J.M., Horn, I., McDonough, W.F., 2002. Experimental constraints on the sulfide- and chromite-silicate melt partitioning behavior of rhenium and the platinum-group elements. Economic Geology 97, 385–398.
Saunders, A.D., Fitton, J.G., Kerr, A.C., Norry, M.J., Kent, R.W., 1997. The North Atlantic Igneous Province. In: Mahoney, J.J., Coffin, M.F. (Eds.), Large Igneous Provinces: Continental, Oceanic, and Planetary Flood Volcanism. American Geophysical Union, Washington DC.
Smith, J.W., Holwell, D.A., McDonald, I., 2014. Precious and base metal geochemistry and mineralogy of the Grasvally Norite–Pyroxenite–Anothosite (GNPA) member, northern Bushveld Complex, South Africa: implications for a multistage emplacement. Mineralium Deposita 49, 667–692.
Søager, N., Portnyagin, M., Hoernle, K., Holm, P.M., Hauff, F., Garbe-Schönberg, 2015. Olivine major and trace element compositions in Southern Payenia basalts, Argentina: evidence for pyroxenite–peridotite melt mixing in a back-arc setting. Journal of Petrology 56 (8), 1495–1518.

Stephenson, D., Fortey, N.J., Gallagher, M.J., 1983. Polymetallic Mineralisation In Carboniferous Rocks At Hilderston, Near Bathgate, Central Scotland. Mineral Reconnaissance Programme Report No. 68. Natural Environment Research Council.
Stone, P., Floyd, J.D., Barnes, R.P., Lintern, B.C., 1987. A sequential back-arc and foreland basin thrust duplex model for the Southern Uplands of Scotland. Journal of the Geological Society 144, 753–764.
Styles, M.T., Gunn, A.G., Rollin, K.E., 2004. A preliminary study of the PGE in the Late Caledonian Loch Borralan and Loch Ailsh alkaline pyroxenite–syenite complexes, north-west Scotland. Mineralium Deposita 39, 240–255.
Trewin, N.H., 2002. Geology of Scotland. The Geological Society, London.
Upton, B.J.G., Aspen, P., Chapman, N.A., 1983. The upper mantle and deep crust beneath the British Isles: evidence from inclusions in volcanic rocks. Journal of the Geological Society 140, 105–121.
Upton, B.G.J., Aspen, P., Rex, D.C., Melcher, F., Kinny, P., 1998. Lower crustal and possible shallow mantle samples from beneath the Hebrides: evidence from a xenolithic dyke at Gribun, western Mull. Journal of the Geological Society 155, 813–828.
Upton, B.G.J., Stephenson, D., Smedley, P.M., Wallis, S.M., Fitton, J.G., 2004. Carboniferous and Permian magmatism in Scotland. In: Neumann, E.-R., Davies, G.R., Timmerman, M.J., Heeremans, M., Larsen, B.T. (Eds.), Permo-Carboniferous Magmatism and Rifting in Europe. Geological Society, London.
Upton, B.G.J., Downes, H., Kirstein, L.A., Bonadiman, C., Hill, P.G., Ntaflos, T., 2011. The lithospheric mantle and lower crust–mantle relationships under Scotland: a xenolithic perspective. Journal of the Geological Society 168, 873–886.
Von Damm, K.L., 2013. Controls on the chemistry and temporal variability of seafloor hydrothermal fluids. Hydrothermal Systems: Physical, Chemical, Biological, And Geological Interactions.
von Gool, J.A.M., Connelly, J.N., Marker, M., Mengal, F., 2002. The Nagssugtoqidian Orogen of West Greenland: tectonic evolution and regional correlations from a West Greenland perspective. Canadian Journal of Earth Sciences 39, 665–686.
Walker, G.P.L., Ross, J.V., 1954. A xenolithic monchiquite dyke near Glenfinnan, Inverness-shire. Geological Magazine 91, 463–472.
Wang, K.-L., O'Reilly, S.Y., Honda, M., Matsumoto, T., Griffin, W.L., Pearson, N.J., Zhang, M., 2010. Co-rich sulfides in mantle peridotites from Penghu Islands, Taiwan: footprints of Proterozoic mantle plumes under the Cathaysia Block. Journal of Asian Earth Sciences 37, 229–245.
Warren, J.M., Shirey, S.B., 2012. Lead and osmium isotopic constraints on the oceanic mantle from single abyssal peridotite sulfides. Earth and Planetary Science Letters 359–360, 279–293.
Westbrook, G.K., Borradaile, G.J., 1978. The geological significance of magnetic anomlaies in the region of Islay. Scottish Journal of Geology 14, 213–224.
Wittig, N., Webb, M., Pearson, D.G., Dale, C.W., Ottley, C.J., Hutchison, M., Jensen, S.M., Luguet, A., 2010. Formation of the North Atlantic Craton: timing and mechanisms constrained from Re–Os isotope and PGE data of peridotite xenoliths from S.W. Greenland. Chemical Geology 276, 166–187.
Young, B.N., Parsons, I., Threadgould, R., 1994. Carbonatite near the Loch Borralan intrusion, Assynt. Journal of the Geological Society, London 45, 945–954.